The Transverse Structure of the Deuteron with Drell-Yan

D. Keller[1]

[1] *University of Virginia, Charlottesville, VA 22904*

(Dated: May 22, 2020)

We propose to measure neutron and deuteron TMDs which includes the first ever measurement of gluon transversity. The quark transversity distributions of the nucleon are decoupled from the gluon transversity in the Q^2 evolution due to the chiral-odd property in the transversely-polarized target providing a particularly clean probe of gluonic degrees of freedom. This experiment can be performed with the SpinQuest polarized target recently assembled for experiment E1039 and the spectrometer already in place in NM4. This new experimental setup would require minimal modification to the target system. An additional RF-coil is necessary to modulate across the domain of the Larmor frequency to manipulate the solid-state target spin population densities. Dedicated beam-time with this novel target system is required to achieve sufficient precision.

CONTENTS

I. INTRODUCTION

How is the quantum spin built in composite systems? This is the quintessential question of Spin Physics. Efforts to answer this question have resulted in the realization that hadrons and nuclei have an increasingly complex internal structure likely involving quark orbital angular momentum (OAM) as well as gluonic and sea quark contributions. The depth of this structure and dynamics are just more recently beginning to be realized due in large part to novel experimentation. The next generation of spin physics experiments is now driven by a modern understanding of spin and must leverage the techniques and technology developed in recent years to acquire a broader physics reach.

The spin of nucleons and nuclei are well known but how the internal mechanisms of motion and conservation manifest to preserve this fixed quantized spin is still not clear. What is clear is that spin, like mass, appears to be an emergent quantity based on constituent movement and interaction with the vacuum. Since the pivotal results provided by the EMC collaboration [1], the particle physics community has strived to make sense of experimental results leading to extensive theoretical development. Decades of experimental studies on high-energy polarized-hadron reactions have been performed to clarify the origin of spin, mainly through longitudinally-polarized structure functions sparking considerable work on how to decompose the nucleon spin, see reviews [2–6].

Studying the spin structure of the nucleon and nuclei is a complex subject as the internal motion of the partons is relativistic and its non-trivial to define the angular momenta. In addition gluon spin is generally thought to be gauge dependent [7] but there are investigations into quark-gluon spin components and OAM contribution in a gauge invariant way [8]. Considering the nonpeturbative nature of these studies, calculations based solely on first principles of QCD are prohibitively challenging. The parton model [9] illustrates the nucleon as a collection of quasi-free quarks, antiquarks and gluons, with longitudinal momentum distributions described by parton densities. The formalism of collinear factorization directly connects these concept to QCD and provides the foundational framework needed in spin physics but only quantifies structure in a single spatial dimension.

To investigate partons in the plane transverse to the direction of motion of its parent nucleon requires the Generalised Parton Distribution (GPDs) and Transverse Momentum Distributions (TMDs) [10]. For both GPDs and TMDs the relevant scales are in the non-perturbative domain, in contrast to the longitudinal momentum fractions on which all types of parton distributions depend. Subject to kinematics the TMDs and GPDs can contain much more information on non-perturbative phenomena and are critical to the interpretation of spin dependent hadron-hadron and lepton-hadron collisions providing the advantage of a multi-dimensional exploration of the structure of nucleons and nuclei. Through this avenue Spin Physics studies of the strong force in its non-perturbative domain and beyond can also provide insight into color confinement as well as the origin of dynamic mass and charge density. The culmination of Spin Physics has yet to come but ultimately experiments will reveal exactly how partonic interactions manifest into hadronic and nuclear degrees of freedom. The spin decomposition using lattice QCD (LQCD) [11–15] also

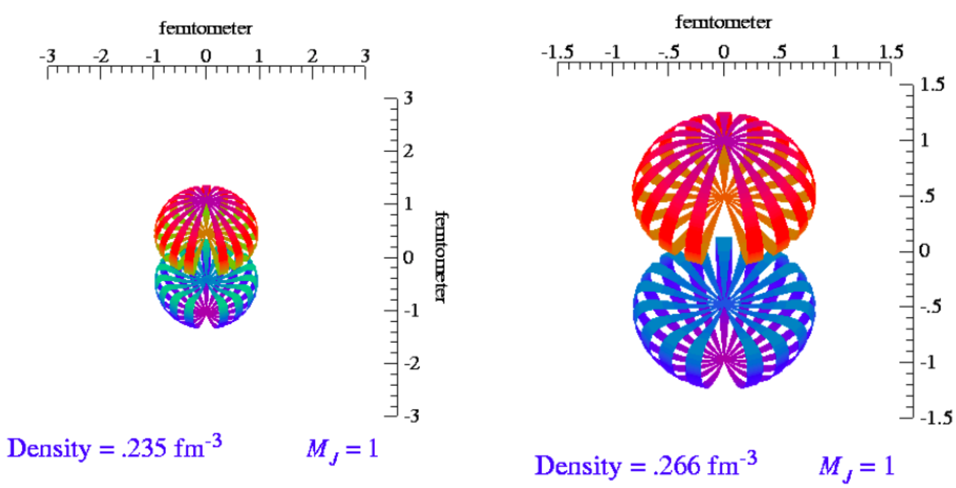

FIG. 1. Graphical representation of the shape of the deuteron for two specified equidensity surfaces. Here the deuteron is in the $M_J = 1$ spin state. The same is similar for $M_J = -1$. Image from Argonne National Lab.

provide a guiding light. Efforts have been made recently to obtain x-dependent parton distributions from LQCD [16]. Calculations of the nucleon spin from first principle simulations are beginning to provide results with control over all systematics [17]. The best determined contributions so far are $\Sigma_q(\frac{1}{2}\Delta q)$ the quark intrinsic spin contribution with quark flavor $(q = u,\ d,\ s,\ c)$, J_q the quark total angular momentum, J_g the gluon total angular momentum, and L_q the OAM of the quarks. The PNMDE [18] collaboration have published results for $\Sigma_q(\frac{1}{2}\Delta q)$ and find $\Sigma_q = 0.143(31)(36)$, consistent with the COMPASS value $0.13<\frac{1}{2}\Delta\Sigma<0.18$ obtained at 3 GeV^2 [19]. The ETMC [20] collaboration has

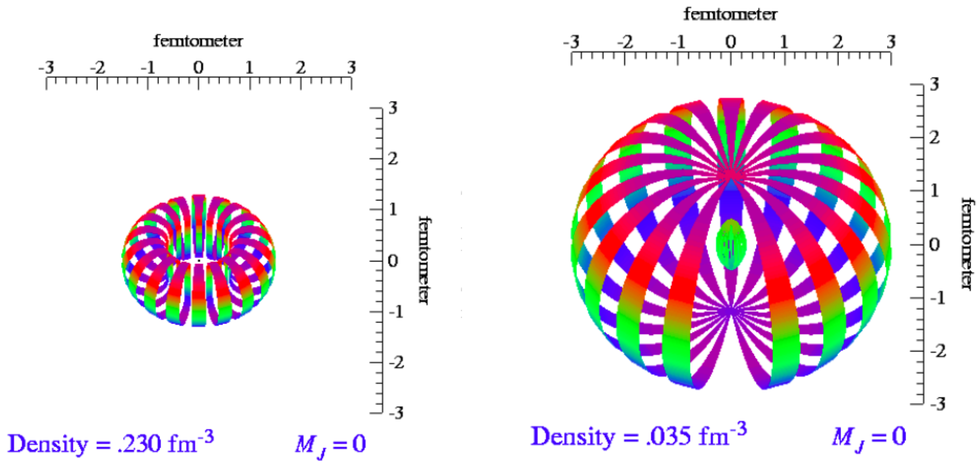

FIG. 2. Graphical representation of the shape of the deuteron for two specified equidensity surfaces. Here the deuteron is in the $M_J = 0$ spin state. Image from Argonne National Lab.

presented first results for J_q and J_g, and L_q [21] for the OAM of quarks. Within the next several years improved high performance computing resources will allow much higher precision LQCD calculations which will require much more experimental information as a basis for comparison. In fact the greatest opportunity to deepen our understand will come form the intersection of consistent results from LQCD, phenomenology and experiments over a broaden range of kinematics.

The next generation of experiments must attempt to measure gluon-spin and partonic OAM contributions, and further explore spin on a composite level by studying nuclei. To extract and understand this information, we need to investigate both the longitudinal spatial structure and the transverse momentum structure using novel methods. Though significant experimental progress has been made adding to the understanding of the spin structure of hadrons, the data frequently leaves more questions to be answered. To understand the spin configuration of the nucleon and nuclei in terms of quarks and gluons remains one of the most challenging and critical open problems in nuclear physics [22, 23]. Vital experimental information is missing especially around the transversely-polarized structure [24–28], with only minimal studies on quark transversity distributions [29]. The transverse polarized target observables provides unique and crucial details on the 3D picture. The internal workings of these observables are distinct from those of the longitudinal structure being the quark transversity distributions are decoupled from the gluon transversity in the Q^2 evolution [30–32] for polarized nuclei with spin $\geq$1 such as the deuteron.

The deuteron is the simplest spin-1 system and offers a vast array of observables to explore as we begin to build the nuclear composite picture. The deuteron initially appears as a loosely bound pair of nucleons with spins aligned (spin triplet state). But the existence of the small quadrupole moment implies that these two nucleons are not in a pure S-state of relative orbital angular momentum, and that the force between them is not central. Taking into account total spin and parity, an additional D-wave component is allowed. There are several layers to understanding this system starting with the tensor force. The deuteron would simply not be bound without the tensor force and there are geometric implications of this force on the deuteron structure which have yet to be explored on the quark and gluon level. The spin configuration and alignment of the deuteron is a tool yet to be taken full advantage of. If a deuteron can be aligned in such a fashion that it is in a $M_J = \pm 1$ magnetic substate (Fig. 1), where J is the spin of the deuteron, then the deuteron can have two separate equidensity surface lobes depending on the energy density. This configuration is associated with the standard spin-up and spin-down common to the spin-1/2 nucleon but for spin-1 it is distinctly referred to as vector polarization. On the other hand if the deuteron is in the $M_J = 0$ magnetic substate (Fig. 2), then the equidensity surfaces that encloses the deuteron are toroidal in shape [33]. The hole in the torus is due of the repulsive core of the N–N interaction and the overall shape is largely governed by the tensor force. It is only recently that the highly control manipulation of a solid-polarized target spin ensemble has allowed access to the optimally aligned high density deuteron targets, allowing increased sensitive to the correlations between geometric properties and partonic degrees degrees of freedom.

We propose the first ever Spin-1 TMD measurements using a polarized deuteron target including a direct measurement of gluon transversity while also for the first time measuring the sea-quark transversity distribution of the deuteron/neutron. The gluon transversity was first mentioned in Deep inelastic scattering [34]. Contributions to this observable vanishes identically for a nucleus made up of protons and neutrons regardless of Fermi motion or binding corrections. It is therefore an unambiguous probe of the gluonic components of the nuclear wavefunction which cannot be identified with individual nucleons. We propose to use the same SpinQuest/E1039 setup using Drell-Yan production from an unpolarized 120 GeV proton beam interacting on a transversely polarized deuteron target. This experiment would use the same exact experimental configuration at Fermilab already setup in NM4. With this new proposal, we suggest implementing polarized target technology in a dedicated run to optimize and separate the tensor polarized observables from the vector contributions making these challenging measurements viable. The unique beam cycle of the high intensity proton beam at Fermilab allows for the employment of special characteristics of the thermal properties of the solid-state polarized target system allowing significant improvement over any other facility to run intense proton beams on novel RF-manipulated target systems. The combination of high luminosity, large x-coverage and a high-intensity beam with significant time between proton spills makes Fermilab ***the best*** place for this novel approach to measuring these polarized target asymmetries in Drell-Yan scattering with high precision. Using the antiquark selectivity of Drell-Yan, we will make the first ever determination of several observables providing multiple constraints and significant advancement in the understanding Spin Physics.

In summary, this new proposal suggests taking full advantage of the new SpinQuest infrastructure by embarking on a spin-physics program to measure multiple polarized observables in the deuteron, within the range of $0.1 < x_B < 0.5$. He we propose for the first time a way to probe exotic gluonic components in the target using transverse momentum distribution function TMDs. This experiment would be highly complementary to the approved experiment E1039 [35], which will measure the Sivers function of the sea quarks using both a polarized proton and deuteron target. The physics presented here is also suggestive of other experiments to gain even further insight. The culmination in information from these experiments will indeed provide remarkable steps forward in the field of High-Energy/Nuclear Spin Physics.

It is important to note that the proposed measurement is the only currently planned experiment which will cleanly access the sea quark and gluon transversity. Fermilab provides a unique and complimentary kinematics with virtuality $Q^2 \sim 10$ GeV^2 and transverse momentum q_T in the few GeV region. This experiment is made possible by the SpinQuest polarized target and supporting infrastructure as well as the technology that is required to optimize the deuteron target to achieve linearly polarized gluons. It is necessary to measure the vector polarized asymmetry with zero tensor polarization and alternate with the unpolarized target cross section measurement. The technology to achieve these types of RF manipulated target systems has recently been developed at the University of Virginia and would require only small hardware modification to the SpinQuest target. While this project would be a continuation of the SpinQuest experiment, E1039 does not use a target optimized for linearly polarized gluons. All of the recent modification in the NM4 experimental hall are required. The installation of the polarized target and closed loop liquid helium system as well as the modifications to the beamline to protect the target superconducting coils, changes to the shielding around the target area and the first magnet are all still necessary in the exact same way for the proposed experiment. There are no additional installations costs required for the proposed run.

II. MOTIVATION

A. The Spin-1 Target in Drell-Yan

High energy scattering experiments are required to probe the quark and gluon structure of hadrons and hadronization processes. This makes parton distribution functions (PDFs) and fragmentation functions (FFs) crucial ingredients in hadron and particle physics [1–3]. Recently, transverse-momentum-dependent quark distribution functions (TMDs) and fragmentation functions (TMD FFs) have been of significant focus both experimentally and theoretically [4–6]. At leading-twist the internal transverse-momentum-dependent quark structure of spin-half hadrons, such as the nucleon, is expressed in terms of six time-reversal even (T-even) and two time-reversal odd (T-odd) TMDs, and after integrating over the transverse momenta of quarks there remain three PDFs: the unpolarized, helicity, and transversity PDFs. However, for spin-one hadrons, such as the deuteron, the spin degrees of freedom require three additional leading-twist T-even TMDs, resulting in one additional PDF [7–9].

The Drell-Yan process [36] describes the hadron-hadron collisions, where at tree level a quark from one particle annihilates with an antiquark from the other particle, creating a virtual photon. The virtual photon subsequently decays into two leptons. The Drell-Yan process is one of the cornerstone perturbative QCD processes that cleanly probes the internal structure of the colliding hadrons, has low background, and is free of the fragmentation uncertainties.

For this proposed experiment we will use $p + d^{\uparrow} \rightarrow \mu^+ + \mu^- + X$ with a transverse vertically pointing deuteron. To lowest order, the cross section for the Drell-Yan process depends on the product of the quark and antiquark distributions q, $\bar{q}$ in the beam x_1 and in the target x_2, where x_1, x_2 are the Bjorken-x of the process and express the fraction of the longitudinal momentum of the hadron carried by the quark.

$$\frac{d\sigma}{dx_1 dx_2} = \frac{4\pi\alpha^2}{9sx_1x_2} \sum_i e_i^2 (q_i^B(x_1, Q^2)\bar{q}_i^T(x_2, Q^2) + \bar{q}_i^B(x_1, Q^2) q_i^T(x_2, Q^2) \ , \tag{1}$$

where s is the square of the center of mass energy and is given by $s = 2m_T E_{Beam} + m_T^2 + m_B^2$, with E_{Beam} as the beam energy and $m_{B,T}$ the rest masses of the beam and target particles. Measuring the two decay leptons in the spectrometer allows one to determine the virtual photon center of mass momentum $p_{\parallel}^{\gamma}$ (longitudinal) and p_T^{γ} (transverse) as well as the mass M_γ. From these quantities one can deduce the momentum fractions of the quarks through:

$$x_F = \frac{p_{\parallel}^{\gamma}}{p_{\parallel}^{\gamma,max}} = x_1 - x_2\,, \qquad x_1 x_2 = M_\gamma^2\,. \tag{2}$$

If one chooses the kinematics of the experiment such that $x_F > 0$ and x_1 is large, the contributions from the valence quarks in the beam dominate.

In this case, in equation 1 the second term becomes negligible and the cross section can be written as

$$\frac{d\sigma}{dx_1 dx_2} \approx \frac{4\pi\alpha^2}{9 s x_1 x_2} \sum_i e_i^2 q_i^B(x_1, Q^2)\bar{q}_i^T(x_2, Q^2)\,. \tag{3}$$

For a proton beam on a proton target the process is dominated by the $u(x_1)$ distribution due to the charge factor e_i^2. But on the neutron (deuteron) target the process is $d(x_1)$ dominant. To explore the sea-quark observables in the neutron we consider the general form of the hadronic tensor from [37] to express the full angular distribution of the Drell-Yan cross section as.

$$\begin{aligned}
d\sigma d^4q d\Omega = \frac{\alpha_{em}^2}{Fq^2} \times \Big\{ & \Big(\left(1+\cos^2\theta\right) F_{UU}^1 + \left(1-\cos^2\theta\right) F_{UU}^2 + \sin 2\theta \cos\phi F_{UU}^{\cos\phi} + \sin^2\theta \cos 2\phi F_{UU}^{\cos 2\phi}\Big) \\
& + S_{aL}\Big(\sin 2\theta \sin\phi F_{LU}^{\sin\phi} + \sin^2\theta \sin 2\phi F_{LU}^{\sin 2\phi}\Big) \\
& + S_{bL}\Big(\sin 2\theta \sin\phi F_{UL}^{\sin\phi} + \sin^2\theta \sin 2\phi F_{UL}^{\sin 2\phi}\Big) \\
+ \left|\vec{S}_{aT}\right| \Big[\sin\phi_a & \Big(\left(1+\cos^2\theta\right) F_{TU}^1 + \left(1-\cos^2\theta\right) F_{TU}^2 + \sin 2\theta \cos\phi F_{TU}^{\cos\phi} + \sin^2\theta \cos 2\phi F_{TU}^{\cos 2\phi}\Big) \\
& + \cos\phi_a \Big(\sin 2\theta \sin\phi F_{TU}^{\sin\phi} + \sin^2\theta \sin 2\phi F_{TU}^{\sin 2\phi}\Big)\Big] \\
+ \left|\vec{S}_{bT}\right| \Big[\sin\phi_b & \Big(\left(1+\cos^2\theta\right) F_{UT}^1 + \left(1-\cos^2\theta\right) F_{UT}^2 + \sin 2\theta \cos\phi F_{UT}^{\cos\phi} + \sin^2\theta \cos 2\phi F_{UT}^{\cos 2\phi}\Big) \\
& + \cos\phi_b \Big(\sin 2\theta \sin\phi F_{UT}^{\sin\phi} + \sin^2\theta \sin 2\phi F_{UT}^{\sin 2\phi}\Big)\Big] \\
+ S_{aL} S_{bL} & \Big(\left(1+\cos^2\theta\right) F_{LL}^1 + \left(1-\cos^2\theta\right) F_{LL}^2 + \sin 2\theta \cos\phi F_{LL}^{\cos\phi} + \sin^2\theta \cos 2\phi F_{LL}^{\cos 2\phi}\Big) \\
+ \left|\vec{S}_{aT}\right| S_{bL} \Big[\cos\phi_a & \Big(\left(1+\cos^2\theta\right) F_{TL}^1 + \left(1-\cos^2\theta\right) F_{TL}^2 + \sin 2\theta \cos\phi F_{TL}^{\cos\phi} + \sin^2\theta \cos 2\phi F_{TL}^{\cos 2\phi}\Big) \\
& + \sin\phi_a \Big(\sin 2\theta \sin\phi F_{TL}^{\sin\phi} + \sin^2\theta \sin 2\phi F_{TL}^{\sin 2\phi}\Big)\Big] \\
+ S_{aL}\left|\vec{S}_{bT}\right| \Big[\cos\phi_b & \Big(\left(1+\cos^2\theta\right) F_{LT}^1 + \left(1-\cos^2\theta\right) F_{LT}^2 + \sin 2\theta \cos\phi F_{LT}^{\cos\phi} + \sin^2\theta \cos 2\phi F_{LT}^{\cos 2\phi}\Big) \\
& + \sin\phi_b \Big(\sin 2\theta \sin\phi F_{LT}^{\sin\phi} + \sin^2\theta \sin 2\phi F_{LT}^{\sin 2\phi}\Big)\Big] + \\
\left|\vec{S}_{aT}\right|\left|\vec{S}_{bT}\right| \Big[\cos\left(\phi_a+\phi_b\right) & \Big(\left(1+\cos^2\theta\right) F_{TT}^1 + \left(1-\cos^2\theta\right) F_{TT}^2 + \sin 2\theta \cos\phi F_{TT}^{\cos\phi} + \sin^2\theta \cos 2\phi F_{TT}^{\cos 2\phi}\Big) \\
+ \cos\left(\phi_a-\phi_b\right) & \Big(\left(1+\cos^2\theta\right) \bar{F}_{TT}^1 + \left(1-\cos^2\theta\right) \bar{F}_{TT}^2 + \sin 2\theta \cos\phi \bar{F}_{TT}^{\cos\phi} + \sin^2\theta \cos 2\phi \bar{F}_{TT}^{\cos 2\phi}\Big) \\
& + \sin\left(\phi_a+\phi_b\right) \Big(\sin 2\theta \sin\phi F_{TT}^{\sin\phi} + \sin^2\theta \sin 2\phi F_{TT}^{\sin 2\phi}\Big) \\
& + \sin\left(\phi_a-\phi_b\right) \Big(\sin 2\theta \sin\phi \bar{F}_{TT}^{\sin\phi} + \sin^2\theta \sin 2\phi \bar{F}_{TT}^{\sin 2\phi}\Big)\Big]\Big\}\,.
\end{aligned}$$

Here there are 48 structure functions that can play some type of role in the observables. In order to shorten the notation the indices for the angles which characterize the lepton momenta and the transverse spin vectors of the hadrons are left out. Also the components of the spin vectors can be understood in different frames like the rest frame of one of the hadrons, the cm-frame, or a dilepton rest frame. For the additional structure function that surface from the spin-1 target see [38–43].

Summing over the polarizations of the produced leptons, the expression for the cross section DY lepton-pair production off a transversely polarized nucleon containing the five transverse spin-dependent asymmetries. This part of the differential cross section can be expressed as [44],

$$\frac{d\sigma}{dq^4 d\Omega} \propto \hat{\sigma}_U \Big\{1 + S_T \Big[D_1 A_T^{\sin\varphi_s} \sin\varphi_s \; + D_2 \Big(A_T^{\sin(2\varphi_{cs}-\varphi_s)} \sin\left(2\varphi_{cs}-\varphi_s\right) \; + A_T^{\sin(2\varphi_{cs}+\varphi_{cs})} \sin\left(2\varphi_{cs}+\varphi_s\right)\Big)\Big]\Big\} \tag{4}$$

where q is the four-momentum of the virtual photon and $\hat{\sigma}_U = (F_U^1 + F_U^2)(1 + \lambda\cos^2\theta_{cs})$, and F_U^1, F_U^2 are the polarization and azimuth-independent structure function, and polar asymmetry λ is given as $\lambda = (F_U^1 - F_U^2)/(F_U^1 + F_U^2)$. $D_1 = (1+\cos^2\theta_{cs})/(1+\cos^2\theta_{cs})$ and $D_2 = \sin^2\theta_{cs}/(1+\cos^2\theta_{cs})$. The angles φ_{cs}, θ_{cs} and Ω the solid angle of the lepton, are defined in the Collins-Soper frame [37]. Naturally, S_T is the transverse part of the nucleon spin.

With the deuteron one can measure observables from both the spin-1/2 neutron and the spin-1 deuteron. To extract the Spin-1 transverse TMDs one has to measure $p+d^{\uparrow}$ transverse spin asymmetry with the target either in the vector or tensor polarization. The polarization of the solid-state target can be manipulated with RF-techniques. The RF spin manipulation to enhance the target for a particular observable can be achieve in-between beam spills optimizing the figure of merit for the beam-target interaction time. The time between beam spills is an advantage in this case allowing time to selectively configure the target to isolate specific sea-quark and gluon observables of interest using novel RF polarized target techniques. The time between beam spills also allows target spin flips per spill reducing the time-dependant drifts in the target asymmetry measurements.

In Drell-Yan lepton-pair production with transversely polarized nucleons in the initial state, the TSA $A_T^{\sin\varphi_s}$ is related to the Sivers TMD by a convolution and the QCD predicted sign-change can be measured in the Drell-Yan process when compared at the same kinematics to the semi-inclusive deep inelastic scattering process (SIDIS). The other two, $A_T^{\sin(2\varphi_{cs}-\varphi_s)}$ and $A_T^{\sin(2\varphi_{cs}+\varphi_s)}$, are related to convolutions of the beam Boer-Mulders ($h_1^{\perp}$) and the target transversity (h_1) or pretzelosity ($h_{1T}^{\perp}$) such that,

$$\text{Boer-Mulders} \otimes \text{Boer-Mulders}: \quad A_T^{\cos 2\varphi_{cs}} \propto h_1^{\perp q} \otimes h_1^{\perp q} \tag{5}$$

$$\text{Unpolarized} \otimes \text{Sivers}: \quad A_T^{\sin\varphi_s} \propto f_1^{q} \otimes f_{1T}^{\perp q} \tag{6}$$

$$\text{Boer-Mulders} \otimes \text{Transversity}: \quad A_T^{\sin(2\varphi_{cs}-\varphi_s)} \propto h_1^{\perp q} \otimes h_1^{q} \tag{7}$$

$$\text{Boer-Mulders} \otimes \text{Pretzelosity}: \quad A_T^{\sin(2\varphi_{cs}+\varphi_s)} \propto h_1^{\perp q} \otimes h_{1T}^{\perp q}. \tag{8}$$

Combined with the kinematic information and the target polarization we can access the TMDs given the experimental asymmetries. Specifically for a vector polarized deuteron target at SpinQuest we can get access to the sea-quark transversity by [45],

$$A_{UT}^{\sin(\phi+\phi_s)\frac{q_T}{M_N}}\Big|_{pD^{\uparrow}\to l^+l^-X} \simeq -\frac{\left[4h_{1u}^{\perp(1)}\left(x_p\right)+h_{1d}^{\perp(1)}\left(x_p\right)\right]\left[\bar{h}_{1u}\left(x_{D^{\uparrow}}\right)+\bar{h}_{1d}\left(x_{D^{\uparrow}}\right)\right]}{\left[4f_{1u}\left(x_p\right)+f_{1d}\left(x_p\right)\right]\left[\bar{f}_{1u}\left(x_{D^{\uparrow}}\right)+\bar{f}_{1d}\left(x_{D^{\uparrow}}\right)\right]}. \tag{9}$$

Here the Boer-Mulders function ($h_1^{\perp q}$) portion can also be measured in the $\cos(2\varphi_{cs})$ term of the unpolarized Drell-Yan measurement [46]. Using the deuteron target provides a cleaner probe to the $\bar{d}$-quark transversity $\bar{h}_{1d}$. This is a primary motivation of this proposal and physically represents the $\bar{d}$-quark polarization in the transversely vector polarized deuteron. To optimize such an experiment the target should be only vector polarized in the transverse vertical direction unlike the standard Boltzmann equilibrium spin configured deuteron target required for SpinQuest E1039 which contains a mix of vector and tensor polarized deuterons. It is necessary to mitigate contamination from the tensor polarized observables to isolate quark contribution to the TSA. Such a target requires special treatment and is discussed later.

Unlike the Sivers function [35] the transversity and pretzelosity are predicted to exhibit true universality, and do not have a sign-change between SIDIS and Drell-Yan. Tests of universality provide a set of fundamental QCD predictions that must be checked experimentally. These relations are,

$$h_1^{q}|_{SDIS} = h_1^{q}|_{DY} \tag{10}$$

$$h_{1T}^{\perp q}\Big|_{SDIS} = h_{1T}^{\perp q}\Big|_{DY} \tag{11}$$

$$h_1^{\perp q}\Big|_{SIDIS} = -\,h_1^{\perp q}\Big|_{DY} \tag{12}$$

$$f_{1T}^{\perp q}\Big|_{SDIS} = -\,f_{1T}^{\perp q}\Big|_{DY}. \tag{13}$$

With the combined experimental data from E1039, and this proposed measurements all of the Drell-Yan portions of these relations can be measured specifically for the sea-quarks. There are no other experiments that can directly measure the sea-quark contribution so this data will be essential for separating the sea and valance contribution for global fits and deepening our general understanding.

In being consistent with the popular work on the subject the subscript U is used to denote unpolarized hadrons, the subscript L and T is used to denote respectively longitudinal and transverse vector polarization and the subscripts LL, LT and TT to denote longitudinal-longitudinal, longitudinal-transverse and transverse-transverse tensor polarization. The tensor polarizations have double index indicating a specific orientation of the tensor polarized state ($m_s = 0$) of the spin-1 target. It is also necessary to use superscripts to indicate which axis is the axis of quantization. For example S_{LL} is the longitudinal component of the spin tensor and it is oriented longitudinally along the z-axis or the beam-line. However, the S_{TL}^{x} term indicates a tensor polarization pointed $\pi/4$ with respect to the beam line in the xz-plane where the x-axis is pointing directly vertical transverse to the beam-line and the y-axis is pointing sideways transverse to the beam-line. With this notation in mind the density matrix is parameterized in terms of a spacelike spin vector S and a symmetric traceless spin tensor T [47]:

$$S^{\mu} = S_L\frac{P^{\mu}}{M} + S_T^{\mu} - MS_Ln^{\mu} \tag{14}$$

and,

$$T^{\mu\nu} = \frac{1}{2}\left[\frac{2}{3}S_{LL}g_T^{\mu\nu} + \frac{4}{3}S_{LL}\frac{P^\mu P^\nu}{M^2} + \frac{S_{LT}^{\{\mu}P^{\nu\}}}{M} + S_{TT}^{\mu\nu} - \frac{4}{3}S_{LL}P^{\{\mu}n^{\nu\}} - MS_{LT}^{\{\mu}n^{\nu\}} + \frac{4}{3}M^2 S_{LL}n^\mu n^\nu\right] \quad (15)$$

In Drell–Yan processes the transverse motion of quarks in nucleons is particularly important, we measure the transverse momentum of a particle that inherits part of the quark intrinsic transverse momentum. The quark momentum is given as,

$$k^\mu \approx xP^\mu + k_T^\mu$$

The most general form of the correlation matrix can be expressed as [27],

$$\Phi(k,P,S) = \frac{1}{2}\left[A_1 \not{P} + A_2\lambda_N\gamma_5 \not{P} + A_3 \not{P}\gamma_5 \not{s}_{\rm T}\right] \quad (16)$$

When the correlation matrix is integrated of k the result gives,

$$\Phi = \int \mathrm{d}^4k\Phi(k,P,S) = \frac{1}{2}\left[g_{\rm V} \not{p} + g_{\rm A}\lambda_N\gamma_5 \not{P} + g_{\rm T} \not{P}\gamma_5 \not{s}_{\rm T}\right] \quad (17)$$

where the constants g_v, g_A and g_T are the vector, axial and tensor charge. The vector charge is the valence number. There can be calculated from the quark and anitquark distribution functions,

$$\begin{aligned} g_{\rm V}^q &= \int_0^1 \mathrm{d}x\left[f_1^q(x) - f_1^{\bar{q}}(x)\right] \\ g_{\rm A}^q &= \int_0^1 \mathrm{d}x\left[g_1^q(x) + g_1^{\bar{q}}(x)\right] \\ g_{\rm T}^q &= \int_0^1 \mathrm{d}x\left[h_1^q(x) - h_1^{\bar{q}}(x)\right]. \end{aligned} \quad (18)$$

The description of the quark-quark correlation matrix at leading twist is,

$$\begin{aligned} \Phi = \frac{1}{2}[& \not{p}A_1 + \varepsilon_{\mu\nu\rho\sigma}\gamma^\mu\frac{P^\nu k_{\rm T}^\rho S_{\rm T}^\sigma}{M}\tilde{A}_1 \\ & + \lambda_N\gamma_5 \not{P}A_2 + \frac{k_{\rm T}\cdot S_{\rm T}}{M}\gamma_5 \not{p}\tilde{A}_2 \\ & + \not{P}\gamma_5 \not{\gamma} A_3 + \frac{k_{\rm T}\cdot S_{\rm T}}{M^2} \not{p}_{\gamma_5}k_{\rm T}\tilde{A}_3 + \frac{\lambda_N}{M} \not{P}\gamma_5 k_{\rm T}\tilde{A}_4 \\ & + \varepsilon_{\mu\nu\rho\sigma}\gamma^\mu\gamma^\nu\gamma_5\frac{P^\rho k_{\rm T}^\sigma}{M}\tilde{A}_5\Big] \end{aligned} \quad (19)$$

In total, the matrix is described by 8 functions where A_n and $\tilde{A}_n$ are real parameters used to simplify the characterization [48]. Powers of the nucleon mass M are present to keep the functions dimensionless. And considering the quark transverse polarization S_T. The transversity and pretzelosity determine the transverse polarization distribution of quarks in a transversely polarized nucleon. From Fig. 3 show quarks in a nucleon polarized along the y-axis may be polarized in all transverse directions depending on their momentum.

Considering the deuteron polarization the density matrix takes the form:

$$\rho(S,T) = \tfrac{1}{3}\left(I + \tfrac{3}{2}S^i\Sigma^i + 3T^{ij}\Sigma^{ij}\right) \quad (20)$$

$$= \begin{pmatrix} \frac{1}{3} + \frac{S_L}{2} + \frac{S_{LL}}{3} & \frac{S_T^x - iS_T^y}{2\sqrt{2}} + \frac{S_{LT}^x - iS_{LT}^y}{2\sqrt{2}} & \frac{S_{TT}^{xx} - iS_{TT}^{xy}}{2} \\ \frac{S_T^{x+iS_T^y}}{2\sqrt{2}} + \frac{S_{LT}^x + iS_{LT}^y}{2\sqrt{2}} & \frac{1}{3} - \frac{2S_{LL}}{3} & \frac{S_T^x - iS_T^y}{2\sqrt{2}} - \frac{S_{LT}^x - iS_{LT}^y}{2\sqrt{2}} \\ \frac{S_{TT}^{xx} + iS_{TT}^{xy}}{2} & \frac{S_T^x + iS_T^y}{2\sqrt{2}} - \frac{S_{LT}^x + iS_{LT}^y}{2\sqrt{2}} & \frac{1}{3} - \frac{S_L}{2} + \frac{S_{LL}}{3} \end{pmatrix} \quad (21)$$

In this proposal we are concerned with both quarks and gluons. For parametrization of the quarks the leading-twist TMD correlator is,

$$\begin{aligned} \Phi\left(x,\boldsymbol{k}_T\right) &\equiv \Phi^{[U]}\left(x,\boldsymbol{k}_T;n,P,S,T\right) \\ &\equiv \int\frac{d(\xi\cdot P)d^2\boldsymbol{k}_T}{(2\pi)^3}e^{ik\cdot\xi}\langle P,S,T|\bar{\psi}(0)U(0,\xi)\psi(\xi)|P,S,T\rangle\Big|_{\xi^+=0}. \end{aligned} \quad (22)$$

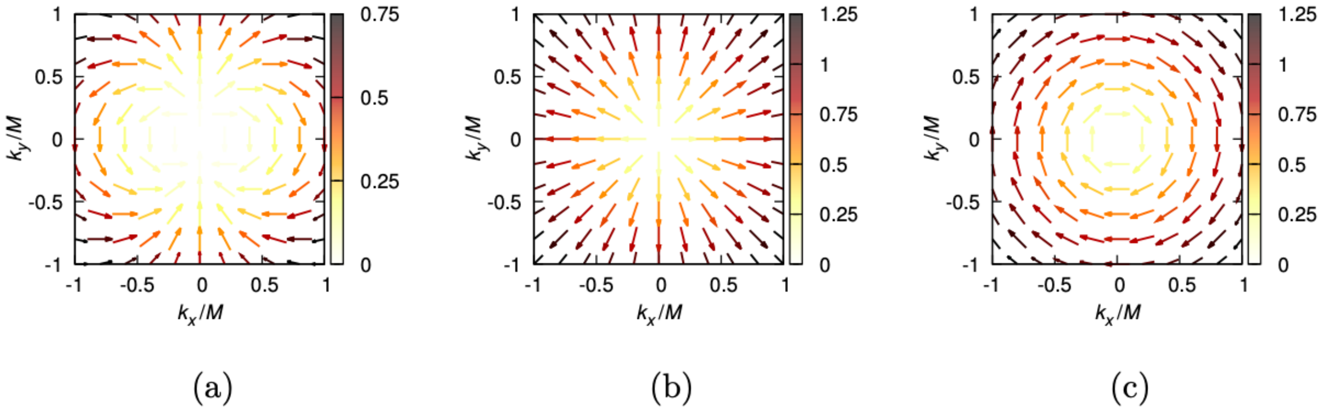

FIG. 3. The kinematic factors accompanying $h^{\perp}{}_{1T}(a)$, $\mathrm{h}_{1L}^{\perp}$(b), and $h_1^{\perp}$(c) for $(\boldsymbol{S}) = (0,1,0)$. Position of the center of each arrow corresponds to the quark transverse momentum, its direction denotes the preferred quark polarization, and the color shows the modulus of the factor [48].

Using the indicated notation the quark correlator is organized in terms of target polarization such that,

$$\Phi = \Phi_U + \Phi_L + \Phi_T + \Phi_{LL} + \Phi_{LT} + \Phi_{TT},$$

and the decomposition is expressed as:

$$\begin{aligned}
\Phi_U\left(x,\boldsymbol{p}_T\right) =& \frac{1}{4}\left\{ f_1\left(x,p_T^2\right)\, \not{n}_+ + \left(h_1^{\perp}\left(x,p_T^2\right)\sigma_{\mu\nu}\frac{p_T^{\mu}}{M}n_+^{\nu}\right)\right\} \\
\Phi_L\left(x,\boldsymbol{p}_T\right) =& \frac{1}{4}\left\{ g_{1L}\left(x,p_T^2\right)S_L\gamma_5\, \not{n}_+ + h_{1L}^{\perp}\left(x,p_T^2\right)S_L\ \mathrm{i}\ \sigma_{\mu\nu}\gamma_5 n_+^{\mu}\frac{p_T^{\nu}}{M}\right\} \\
\Phi_T\left(x,\boldsymbol{p}_T\right) =& \frac{1}{4}\left\{ g_{1T}\left(x,p_T^2\right)\frac{\boldsymbol{S}_T\cdot\boldsymbol{p}_T}{M}\gamma_5\, \not{n}_+ + h_{1T}\left(x,p_T^2\right)\mathrm{i}\sigma_{\mu\nu}\gamma_5 n_+^{\mu}S_T^{\nu}\right. \\
&+ h_{1T}^{\perp}\left(x,p_T^2\right)\frac{\boldsymbol{S}_T\cdot\boldsymbol{p}_T}{M}\mathrm{i}\sigma_{\mu\nu}\gamma_5 n_+^{\mu}\frac{p_T^{\nu}}{M} \\
&\left.+ \left(f_{1T}^{\perp}\left(x,p_T^2\right)\epsilon_{\mu\nu\rho\sigma}\gamma^{\mu}n_+^{\nu}\frac{p_T^{\rho}}{M}S_T^{\sigma}\right)\right\} \\
\Phi_{LL}\left(x,\boldsymbol{p}_T\right) =& \frac{1}{4}\left\{ f_{1LL}\left(x,p_T^2\right)S_{LL}\, \not{n}_+ + \left(h_{1LL}^{\perp}\left(x,p_T^2\right)S_{LL}\sigma_{\mu\nu}\frac{p_T^{\mu}}{M}n_+^{\nu}\right)\right\} \\
\Phi_{LT}\left(x,\boldsymbol{p}_T\right) =& \frac{1}{4}\left\{ f_{1LT}\left(x,p_T^2\right)\frac{\boldsymbol{S}_{LT}\cdot\boldsymbol{p}_T}{M}\, \not{n}_+ + \left(g_{1LT}\left(x,p_T^2\right)\epsilon_T^{\mu\nu}S_{LT\mu}\frac{p_{T\nu}}{M}\gamma_5\, \not{n}_+\right)\right. \\
&+ \left(h_{1LT}'\left(x,p_T^2\right)\mathrm{i}\sigma_{\mu\nu}\gamma_5 n_+^{\mu}\epsilon_T^{\nu\rho}S_{LT\rho}\right) \\
&\left.+ \left(h_{1LT}^{\perp}\left(x,p_T^2\right)\frac{\boldsymbol{S}_{LT}\cdot\boldsymbol{p}_T}{M}\sigma_{\mu\nu}\frac{p_T^{\mu}}{M}n_+^{\nu}\right)\right\}
\end{aligned}$$

$$\begin{aligned}
\Phi_{TT}\left(x,\boldsymbol{p}_T\right) = \frac{1}{4}&\left\{ f_{1TT}\left(x,p_T^2\right)\frac{\boldsymbol{p}_T\cdot\boldsymbol{S}_{TT}\cdot\boldsymbol{p}_T}{M^2}\, \not{n}_+\right. \\
&- \left(g_{1TT}\left(x,p_T^2\right)\epsilon_T^{\mu\nu}S_{TT\nu\rho}\frac{p_T^2 p_{T\mu}}{M^2}\gamma_5\, \not{n}_+\right) \\
&- \left(h_{1TT}'\left(x,p_T^2\right)\mathrm{i}\sigma_{\mu\nu}\gamma_5 n_+^{\mu}\epsilon_T^{\nu\rho}S_{TT}\rho p_{\sigma}\frac{p_T^{\sigma}}{M}\right) \\
&\left.+ \left(h_{1TT}^{\perp}\left(x,p_T^2\right)\frac{\boldsymbol{p}_T\cdot\boldsymbol{S}_{TT}\cdot\boldsymbol{p}_T}{M^2}\sigma_{\mu\nu}\frac{p_T^{\mu}}{M}n_+^{\nu}\right)\right\}.
\end{aligned}$$

In regards to the phenomenology, the intrinsic motion of partons inside the nucleons is responsible for the specific dependence of the cross section in the azimuthal angle. The various correlations encoded in the TMDs translate into the aforementioned azimuthal or spin asymmetries of the measured cross section, which are calculable and provide the basis for measurements giving access to a physical interpretation of structure and dynamics.

The unpolarized TMD f_1 is quite well known now which is good because it is critical to the interpretation of other measurements. The data on the unpolarized function are extracted from facilities worldwide. For the valance quarks Sivers function $f_{1T}^{\perp}$ there is also increasingly more information. SpinQuest E1039 will make a critical contribution for sea quarks. Some information exists on valance quark transversity h_1 and the Boer-Mulders $h_1^{\perp}$ function as well as the pretzelosity h^{1T} [49] but considerably less for the sea. Beyond this there is essential no experimental information on any of the other functions. In Fig. 4 the list is shown of leading twist quark TMDs for the spin-1 target which contain 3 additional T-even and 7 additional T-odd TMDs compared to spin-1/2 nucleons. The rows indicate target polarization and the columns indicate quark polarization. The bold-face functions survive integration over transverse momenta.

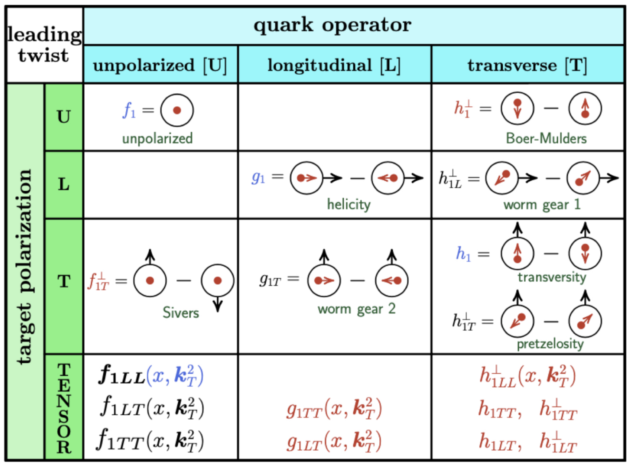

FIG. 4. The list of leading twist quark TMDs for the spin-1 target which contain 3 additional T-even and 7 additional T-odd TMDs compared to spin-1/2 nucleons. The Gluon TMDs are listed in Fig. 5. Here the rows indicate target polarization and the columns indicate quark polarization. The bold-face functions survive integration over transverse momenta.

Naturally valence quarks have been the focus for the last few decades. There has been considerable theoretical effort in the last several year to understand the gluonic content of hadrons. Gluon observables can be easily overwhelmed by the valence quarks depending on the target and the kinematics available at the facility. However, the structure and dynamics produced by the the gluons and the quark sea are turning out to be critical to answer many pressing questions and they must be studied in detail.

As there is a clear need for sea quark specific experiments, the information on gluon distributions is far more scarce and essentially restricted to the collinear gluon PDFs for spin-1/2 targets. Gluon TMDs are mostly unknown because it is generally challenging to access the relevant kinematic regions for a spin-1/2 target. What little information that is available on gluons comes from the LHC at CERN.

Little GPD or TMD information is available on spin-1 targets and absolutely no experimental information is available on the tensor polarization contributions in TMDs. However, the interest on the gluon content of nuclei is growing, even if restricted to the collinear quantities. The collinear structure function for gluons in spin-1 targets was first defined by Jaffe and Manohar [34] and referred as nuclear gluonometry. This observable is related to a transfer of two units of helicity to the polarized target, and vanishes for any target of spin smaller than 1. A finite value to this observable requires the existence of a tower of gluon operators contributing to the scattering amplitude where such a double-helicity flip cannot be linked to single nucleons. This observable is exclusive to hadrons and nuclei of spin ≥ 1 and measures a gluon distribution in the target providing a clear signature for exotic gluonic components in the target. In the parton model language, this observable comes from the linearly polarized gluons in targets with transverse tensor polarization, and is related to h_{1TT}. This interesting function is the focal point of our motivation and is one of the least investigated aspect in the gluonic structure linked to the polarization of the target of spin$\leq$1, where non-nucleonic dynamics becomes accessible. These tensor polarized observables are expected to yield new insights into the internal dynamics of hadrons and nuclei.

Going beyond the collinear case, one can define new TMDs, Fig 5. These TMDs appear in the parametrization of a TMD correlator, which is a bilocal matrix element containing nonlocal field strength operators and Wilson lines. The Wilson lines, or gauge links, guarantee color gauge invariance by connecting the nonlocality, and give rise to a process dependence of the TMDs. The description of spin-1 TMDs is presented by Bacchetta and Mulders [50] for quarks and Boer*et al.* [47] for gluons. Additionally a study of the properties of and the relations between the gluon TMDs for spin-1 hadrons has recently been published [52]. Positivity bounds were derived that provide model-independent inequalities, that help relating and estimating the magnitude of the gluon TMDs.

In [47] the gluon-gluon TMD correlator was parametrized in terms of TMDs for unpolarized, vector, as well as tensor polarized targets. We use a decomposition for the gluon momentum k in terms of the hadron momentum P and the lightlike four-vector n, such that

$$k^\mu = xP^\mu + k_T^\mu + \left(k \cdot P - xM^2\right) n^\mu,$$

satisfying $P \cdot n = 1$ and $P^2 = M^2$, where M is the mass of the hadron. The gluon-gluon TMD correlator for spin-1 hadrons is defined as:

$$\Gamma^{[U,U']\mu\nu;\rho\sigma}\left(x, \boldsymbol{k}_T, P, n; S, T\right) \equiv \int \frac{d\xi \cdot P d^2\boldsymbol{\xi}_T}{(2\pi)^3} e^{ik\cdot\xi} \left\langle P; S, T \left| \mathrm{Tr}_c \left(F^{\mu\nu}(0) U_{[0,\xi]} F^{\rho\sigma}(\xi) U'_{[\xi,0]} \right) \right| P; S, T \right\rangle \Big|_{\xi\cdot n=0} \tag{23}$$

where the process-dependent Wilson lines $U_{[0,\xi]}$ and $U'_{[0,\xi]}$ are required for color gauge invariance. The leading-twist terms are identified as the ones containing the contraction of the field strength tensor with n and one transverse index ($i, j = 1, 2$). Explicitly indicating the dependence of the vector and tensor part of the spin. The correlator is then expressed as,

$$\Gamma^{ij}\left(x, \boldsymbol{k}_T\right) \equiv \int \frac{d(\xi \cdot P) d^2\boldsymbol{k}_T}{(2\pi)^3} e^{ik\cdot\xi} \left\langle P, S, T \left| F^{\mu\nu}(0) U(0,\xi) F^{\rho\sigma}(\xi) U'(\xi, 0) \right| P, S, T \right\rangle_{\xi^+=0} \tag{24}$$

where there is a trace over color and the dependence on the gauge links is omitted. After the separation in terms of the possible hadronic polarization states, the correlator can be expressed using the indicated notation as the following,

$$\Gamma^{ij} = \Gamma^{ij}_U + \Gamma^{ij}_L + \Gamma^{ij}_T + \Gamma^{ij}_{LL} + \Gamma^{ij}_{LT} + \Gamma^{ij}_{TT}. \tag{25}$$

The parametrization in terms of TMDs with specific polarizations and orientations can then be expressed as,

$$\begin{aligned}
\Gamma^{ij}_U\left(x, \boldsymbol{k}_T\right) &= \tfrac{x}{2}\left[-g_T^{ij} f_1\left(x, \boldsymbol{k}_T^2\right) + \tfrac{k_T^{ij}}{M^2} h_1^\perp\left(x, \boldsymbol{k}_T^2\right)\right] \\
\Gamma^{ij}_L\left(x, \boldsymbol{k}_T\right) &= \tfrac{x}{2}\left[i\epsilon_T^{ij} S_L g_1\left(x, \boldsymbol{k}_T^2\right) + \tfrac{\epsilon_T^{\{i}{}^{\alpha} k_T^{j\}\alpha} S_L}{2M^2} h_{1L}^1\left(x, \boldsymbol{k}_T^2\right)\right] \\
\Gamma^{ij}_T\left(x, \boldsymbol{k}_T\right) &= \tfrac{x}{2}\Bigg[-\tfrac{g_T^{ij}\epsilon_T^{S_T k_T}}{M} f_{1T}^1\left(x, \boldsymbol{k}_T^2\right) + \tfrac{i\epsilon_T^{ij} \boldsymbol{k}_T\cdot\boldsymbol{S}_T}{M} g_{1T}\left(x, \boldsymbol{k}_T^2\right) \\
&\quad - \tfrac{\epsilon_T^{k_T}\left\{i_S^{j\}} + \epsilon_T^{S_T\{i} k_T^{j\}}\right.}{4M} h_1\left(x, \boldsymbol{k}_T^2\right) - \tfrac{\epsilon_T^{\{i}\alpha_T^{j\}\alpha S_T}}{2M^3} h_{1T}^\perp\left(x, \boldsymbol{k}_T^2\right)\Bigg] \\
\Gamma^{ij}_{LL}\left(x, \boldsymbol{k}_T\right) &= \tfrac{x}{2}\left[-g_T^{ij} S_{LL} f_{1LL}\left(x, \boldsymbol{k}_T^2\right) + \tfrac{k_T^{ij} S_{LL}}{M^2} h_{1LL}^\perp\left(x, \boldsymbol{k}_T^2\right)\right] \\
\Gamma^{ij}_{LT}\left(x, \boldsymbol{k}_T\right) &= \tfrac{x}{2}\Bigg[-\tfrac{g_T^{ij} \boldsymbol{k}_T\cdot\boldsymbol{S}_{LT}}{M} f_{1LT}\left(x, \boldsymbol{k}_T^2\right) + \tfrac{i\epsilon_T^{ij}\epsilon_T^{S_{LT} k_T}}{M} g_{1LT}\left(x, \boldsymbol{k}_T^2\right) \\
&\quad + \tfrac{S_{LT}^{\{i} k_T^{j\}}}{M} h_{1LT}\left(x, \boldsymbol{k}_T^2\right) + \tfrac{k_T^{ij\alpha} S_{LT\alpha}}{M^3} h_{1LT}^\perp\left(x, \boldsymbol{k}_T^2\right)\Bigg] \\
\Gamma^{ij}_{TT}\left(x, \boldsymbol{k}_T\right) &= \tfrac{x}{2}\Bigg[-\tfrac{g_T^{ij} k_T^{\alpha\beta} S_{TT\alpha\beta}}{M^2} f_{1TT}\left(x, \boldsymbol{k}_T^2\right) + \tfrac{i\epsilon_T^{ij}\epsilon_{T\gamma}^{\beta} k_T^{\gamma\alpha} S_{TT\alpha\beta}}{M^2} g_{1TT}\left(x, \boldsymbol{k}_T^2\right) \\
&\quad + S_{TT}^{ij} h_{1TT}\left(x, \boldsymbol{k}_T^2\right) + \tfrac{S_{TT\alpha}^{(i)} k_T^{j\}\alpha}}{M^2} h_{1TT}^L\left(x, \boldsymbol{k}_T^2\right) \\
&\quad + \tfrac{k_T^{ij\alpha\beta} S_{TT\alpha\beta}}{M^4} h_{1TT}^{\perp\perp}\left(x, \boldsymbol{k}_T^2\right)\Bigg]
\end{aligned}$$

The resulting list of leading twist TMDs for gluons is shown in Fig. 5. The Gluon TMD functions are divided in terms of target polarization and gluon polarization as shown in the figure. The bold-face functions survive integration over transverse momenta.

The phenomenological studies of gluons generally focus on characterizing the appropriate angular dependencies to access gluon distributions. The extraction of these functions should rely on all-order TMD factorization, even though, for processes initiated by gluons, factorization breaking effects are often present [53–57]. Here complexity can arise in factorization breaking from color entanglement and color-singlet configurations. It is worth pointing out that the extraction of the gluon TMDs from different high energy processes requires taking into account the appropriate gauge link structures. In situations where higher number of hadrons are involved, the gauge links can be combinations of future and past pointing Wilson lines, with the possibility of additional loops [58].

The gluon Sivers function can be studied at RHIC and COMPASS and now Fermilab, which can provide the transverse polarization of the target. The Sivers function can be accessed through the measurement of the Sivers asymmetry in $pp^\uparrow \to \pi X$, and in J/ψ production [59–61]. As far as the universality of the gluon Sivers function is concerned, we should expect a sign-change analogously to the quark case.

Target Polarization	Leading Twist	Gluon Operator: Unpolarized	Circular	Linear
Vector Polarized	U	$\boldsymbol{f_1}$		$h_1^{\perp}$
Vector Polarized	L		$\boldsymbol{g_1}$	$h_{1L}^{\perp}$
Vector Polarized	T	$f_{1T}^{\perp}$	g_{1T}	$h_1, h_{1T}^{\perp}$
Tensor Polarized	LL	$\boldsymbol{f_{1LL}}$		$h_{1LL}^{\perp}$
Tensor Polarized	LT	f_{1LT}	g_{1LT}	$h_{1LT}, h_{1LT}^{\perp}$
Tensor Polarized	TT	f_{1TT}	g_{1TT}	$\boldsymbol{h_{1TT}}$, $h_{1TT}^{\perp}$ $h_{1TT}^{\perp\perp}$

FIG. 5. The list of leading twist TMDs gluons. The rows indicate the target polarization while the columns indicate the gluon polarization. The bold-face functions survive integration over transverse momenta.

The longitudinal tensor polarized TMD f_{LL} can also be measured at Fermilab [62]. This would require a different target magnet which the University of Virginia presently owns. This wold require disassembly and reassembly of the target so it is better to measure everything possible within the transverse case first. In either case These gluon observables relate to a transfer of two units of helicity to the nuclear target, and vanish for any target with spin less than 1. So in that case we focus on the linearly polarized gluons in targets with a transverse tensor polarized target to measure the gluon transversity h_{TT}^{1}.

B. Transversity

The transverse-polarization physics of the deuteron can be investigated by the transversity distributions in the twist-2-level collinear framework. Of specific interest are the sea-quark transversity distribution as well as the gluon transversity. To understand how to access the gluon transversity more explanation is required. The approach to quark transversity on the other hand is relatively well known and some measurements have already been performed on the valance contributions. The proposed experiment would provide essential information for such a test specific to the sea-quarks. Fermilab is unique in its kinematic range providing some overlap with other high-x facilities allowing for the critical tests of universality and much more.

1. *Quark Transversity*

As mentioned, an important channels to investigate the quark transversity distribution is the space-like process to Drell-Yan or SIDIS where it is necessary to measure the Collins azimuthal spin asymmetries in order to extract the TMDs [63, 64]. Measurements have been made by the HERMES Collaboration [65, 66], the COMPASS Collaboration [19] and JLab Hall A [67]. The quark transversity distributions requires the Collins fragmentation functions, which are different from the usual unpolarized fragmentation functions. BELLE and BABAR have attempted some extractions of the observables [68–70]. Due to the universality of the Collins fragmentation function [71] it is possible to constrain the fragmentation function and the valance quark transversity given the multiple data sets and analyses using transversity coupled to the dihadron interference fragmentation functions [72]. There has also been effort to apply the appropriate QCD evolution to the phenomenological studies [73] and improve the global picture of transversity.

In the global fit with TMD evolution there are two unknown functions to be extracted using the experimental data. The collinear transversity distributions h_1^q and the collinear twist-3 fragmentation function $\hat{H}^(3)_{h/q}$. The fit parameterizes [73] the quark transversity distributions as

$$h_1^q\,(x, Q_0) = N_q^h x^{a_q} (1-x)^{b_q} \frac{(a_q + b_q)^{a_q + b_q}}{a_q^{a_q} b_q^{b_q}} \frac{1}{2} \left(f_1^q\,(x, Q_0) + g_1^q\,(x, Q_0)\right) \tag{26}$$

where Q_0 is the initial scale, for up and down quarks $q = u,\ d$, respectively, and f_1^q are the unpolarized CT10NLO quark distributions [74] and the NLO DSSV quark helicity distributions. In this parametrization the so-called Soffer positivity bound [75] of transversity distribution at the initial scale was applied. This bound is known to be valid [32] up to NLO order in perturbative QCD. This study assumes that all the sea-quark transversity distributions are negligible. It is well understood that this is a less than ideal place to start for such an extraction however there is no data for the sea-quark contribution. With more data available from SpinQuest and this proposed experiment, it would be possible to constrain the sea-quarks as well. The resulting extracted transversity distributions for the valance u and d quarks are shown in Fig. 6. Other extractions have been made using the two-hadron production in electron-positron annihilation $e^+e^- \to h_1 h_2 X$ where the Collins effect is observed in the combination of the fragmenting processes of a quark and an antiquark , resulting in the product of two Collins functions with an overall modulation of the azimuthal angles of the final hadrons around the quark-antiquark axis [**?**]. Similarly extraction of the transversity distribution

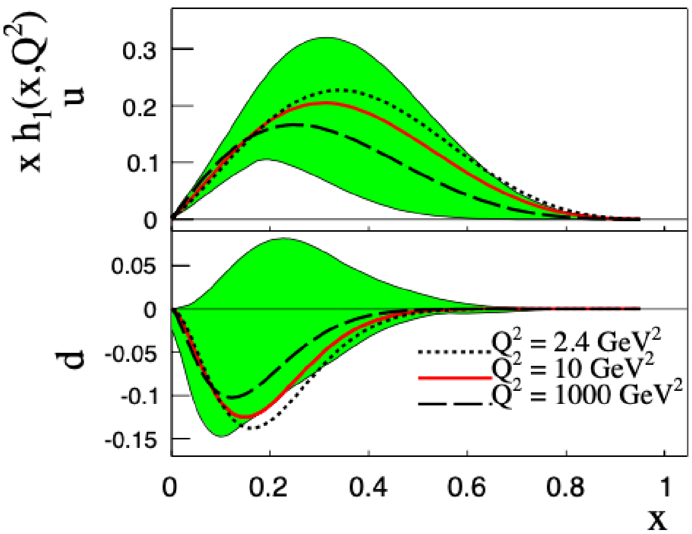

FIG. 6. The extracted transversity distribution at three different scales in Q^2. The shaded region corresponds to the 90% confidence level error band at $Q^2 = 10$ GeV^2 [73].

in the framework of collinear factorization was made based on the global analysis of pion-pair production in deep-inelastic scattering and in proton-proton collisions with a transversely polarized proton [76]. For the transversely polarized nucleon, transversity distributions are expressed as $\Delta Tq(x) = q_\uparrow(x) - q_\downarrow(x)$, where $\uparrow$ and $\downarrow$ indicate parallel and anti-parallel quark polarizations to the transversely-polarized nucleon spin.

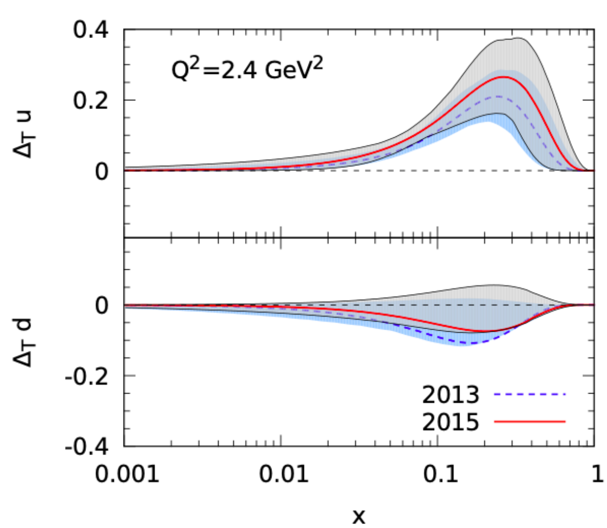

FIG. 7. The extracted u and d transversity distributions in a comparison of the best fit results (red, solid lines). [76].

There has been one attempt made to extract something about the sea-quark contribution [**?**] but this extraction largely lacks constraints for any realistic determination. The results in this case imply the sea-quark transversity is compatible with zero but especially in the case of the $\bar{d}$ there error is simply to large to say anything definite. We will use these results to demonstrate the possible constraints that this proposal could add in the Expected Results section.

To take a closer look at the quark transversity and the physics specific to the deuteron consider that the unpolarized, longitudinally-polarized, and transversity distribution functions are defined for quarks by the following matrix elements [28],

$$q(x) = \int \frac{d\xi^-}{4\pi} e^{ixp^+\xi^-} \left\langle p \left| \bar{\psi}(0)\gamma^+\psi(\xi) \right| p \right\rangle_{\xi^+=\vec{\xi}_\perp=0} \tag{27}$$

$$\Delta q(x) = \int \frac{d\xi^-}{4\pi} e^{ixp^+\xi^-} \left\langle ps_L \left| \bar{\psi}(0)\gamma^+\gamma_5\psi(\xi) \right| ps_L \right\rangle_{\xi^+=\bar{\xi}_\perp=0} \tag{28}$$

$$\Delta_T q(x) = \int \frac{d\xi^-}{4\pi} e^{ixp^+\xi^-} \left\langle ps_{Tj} \left| \bar{\psi}(0)i\gamma_5\sigma^{j+}\psi(\xi) \right| ps_{Tj} \right\rangle_{\xi^+=\bar{\xi}_\perp=0} \tag{29}$$

where s_L and s_{Tj} ($j = 1$ or 2) indicate longitudinal and transverse polarizations of the nucleon, and ψ is the quark field. These distribution functions are leading twist. The structure function gT associated with the transverse spin can be written in an operator matrix element in a similar way as,

$$g_{T,q}(x) = \frac{p^+}{M_N} \int \frac{d\xi^-}{4\pi} e^{ixp^+\xi^-} \left\langle ps_T \left| \bar{\psi}(0)\gamma_\perp\gamma_5\psi(\xi) \right| ps_T \right\rangle_{\xi^+=\bar{\xi}_\perp=0}, \tag{30}$$

which is a twist-3 structure function.

The structure functions of the nucleon are given by the imaginary part of forward scattering amplitudes by the optical theorem. Figure 8 shows the parton-hadron forward scattering amplitudes.

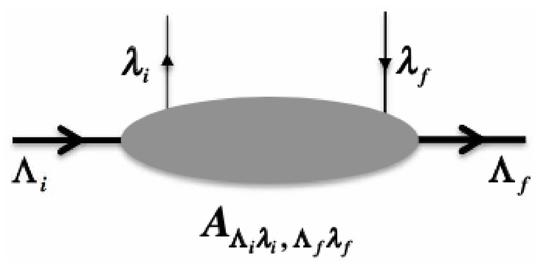

FIG. 8. Parton-hadron forward scattering amplitude $A_{\Lambda_i i,\Lambda_f\lambda_f}$ with the hadron helicities Λ_i and Λ_f and parton helicities λ_i and λ_f.

The amplitude is written as $A_{\Lambda_i i,\Lambda_f\lambda_f}$ with the initial and final hadron helicities Λ_i and Λ_f and with parton helicities λ_i and λ_f such that the PDFs can be related to the helicity amplitudes by [22, 28],

$$\begin{aligned} f_1(x) = q(x) = q_+(x) + q_-(x) \sim \mathrm{Im}\left(A_{++,++} + A_{+-,+-}\right) \\ g_1(x) = \Delta q(x) = q_+(x) - q_-(x) \sim \mathrm{Im}\left(A_{++,++} - A_{+-,+-}\right) \\ -h_1(x) = \Delta_T q(x) = q_\uparrow(x) - q_\downarrow(x) \sim \mathrm{Im}\, A_{++,--}. \end{aligned}$$

where the direction of the polarization is perpendicular to the beam and the amplitudes are defined by the transversely-polarized states so the transversity distribution is

$$\Delta_T q(x) = q_\uparrow(x) - q_\downarrow(x) \sim \mathrm{Im}\left(A_{\uparrow\uparrow,\uparrow\uparrow} - A_{\uparrow\downarrow,\uparrow\downarrow}\right). \tag{31}$$

The SpinQuest polarized target configuration can be used to probe the sea-quark transversity distributions and help in the determination of the tensor charge in the nucleon. The already proposed experiment E1039 will take data on both transversely polarized protons and neutrons but without additional data to separate the vector and tensor polarization contributions the neutron transversity will be very difficult to decipher. This proposal is specific to the control of the deuteron polarization states where a large part of the vector polarization actually comes from the neutron. Transversity is an important physical quantity for clarifying the nature of the nucleon spin and also for exploring possible signatures beyond the standard model [77–79] by observing electric dipole moments of the neutron. There is also considerable theoretical work in lattice QCD [78, 80–88] as well as the Dyson-Schwinger Equation (DSE) [89, 90].

The neutron electromagnetic current can be written as[91–97],

$$\begin{aligned} \left\langle n \left| J_\mu^{\mathrm{em}} \right| n \right\rangle = & \bar{u}\left(p'\right)\left[\gamma_\mu F_1\left(q^2\right) + \frac{\kappa}{2M_N} i\sigma_{\mu\nu}q^\nu F_2\left(q^2\right) \right. \\ & \left. + \frac{d_n}{2M_N}\gamma_5\sigma_{\mu\nu}q^\nu F_3\left(q^2\right)\right] u(p). \end{aligned} \tag{32}$$

Here the time-reversal odd term is included with the form factor F_3 in addition to the ordinary parity and time-reversal even terms with F_1 and F_2 the Dirac and Pauli form factors respectively and κ as the anomalous magnetic moment. The initial and final neutron momenta are denoted as p and p_0, where q is the momentum transfer given by $q = p - p'$, and $u(p)$ is the Dirac spinor for the neutron. Finally F_3 is the time-reversal odd form factor, in combination with the electro-magnetic field A^μ in the Hamiltonian, with the factor of the neutron electric dipole moment (EDM) d_n in units of $e/(2M_n)$.

The nucleon tensor charge is a fundamental nuclear property and its determination is among the main goals of several experiments [98–104]. In terms of the partonic structure of the neutron, the tensor charge, for a particular quark type q, is constructed from the quark transversity distribution, $h_1(x, Q^2)$ [98–102], where the neutron EDM is expressed by integrals of the transversity distributions to obtain the tensor charge,

$$d_n = \sum_q d_q \delta q(Q^2) \tag{33}$$

$$\delta q\left(Q^2\right) \equiv \int_0^1 dx \left(h_1^q\left(x, Q^2\right) - h_1^{\bar{q}}\left(x, Q^2\right)\right) \tag{34}$$

where d_q is the quark EDM. The neutron EDM is investigated theoretically by calculating the quark EDMs in the standard model, or theories that deviate from the standard model. The EDM is multiplied by the tensor charge in order to compare with experimental measurements. The contributions from the sea-quarks to the transversity distributions of the neutron are critical to a detailed understanding and physics interpretation.

2. Gluon Transversity

Equation 31 shows that the transversity distribution $\Delta_T q(x)$ is associated with the quark spin flip ($\lambda_i = +$, $\lambda_f = -$), a chiral-odd distribution. Clearly the gluon transversity can not exist in the nucleon where the spin flip = 2 is not possible. The quark transversity distributions evolve without the corresponding gluon distribution in the nucleon [32] which differs from the longitudinally-polarized PDFs, where the quarks and gluon distributions couple with each other in the Q^2 evolution. This is a subtle yet critical point because it provide a crucial test of the perturbative QCD in Spin Physics.

Similarly to the quark transversity, Eq. 31, the gluon transversity is written as

$$\Delta_T g(x) \sim \mathrm{Im}\, A_{++,--}, \tag{35}$$

where the spin flip of $\Delta s = 2(|\lambda_f - \lambda_i| = |\Lambda_f - \Lambda_i| = 2)$ is necessary for gluon transversity, see Fig 9. The most simple and stable spin-1 hadron or nucleus is the deuteron, which is our choice for the future experiment to study gluon transversity. By angular momentum conservation, the linear polarization of a gluon is zero for the spin-1/2 hadron. Naturally linear polarization is measured by an operator that flips helicity by two units. Since no helicity is absorbed by the space-time part of the definition of the parton densities (the integrals are azimuthally symmetric), the helicity flip in the operator must correspond to a helicity flip term in the density. The gluon correlation function is defined as,

$$\begin{aligned}\Phi^{\alpha\beta}_{g/H}\left(p_h, p_H, s_H\right) =& N_{g/H} \int \frac{d^4\xi}{(2\pi)^4} e^{ip_h\cdot\xi_h} \\ &\times \left\langle p_H s_H \left| A^\alpha(0) A^\beta(\xi) \right| p_H s_H \right\rangle\end{aligned} \tag{36}$$

where A^α is give by $A^\alpha = A^\alpha_a t^\alpha$ and $N_{h/H}$ is the normalization constant. The gluon correlation function in the deuteron at twist-2 is

$$\begin{aligned}&\Phi^{\alpha\beta}_{g/B}\left(x_b\right) \equiv \int d^2 p_{bT} \Phi^{\alpha\beta}_{g/B}\left(x, \vec{p}_{bT}\right) \\ &= \tfrac{1}{2}\left[-g_T^{\alpha\beta} f_{1,g/B}\left(x_b\right) + i\epsilon_T^{\alpha\beta} S_L g_{1,g/B}\left(x_b\right) - g_T^{\alpha\beta} S_{LL} f_{1LL,g/B}\left(x_b\right) + S_{TT}^{\alpha\beta} h_{1TT,g/B}\left(x_b\right)\right]\end{aligned} \tag{37}$$

where $f_{1,g/B}$ is the unpolarized gluon distribution function, $g_1, g/B$ is the longitudinally-polarized distribution function, $f_{1LL,g/B}$ is the longitudinally tensor polarized distribution function and $h_{1TT,g/B}$ is the transversely tensor polarized distribution function or the gluon transversity. It is clear that the matrix elements $S^{\alpha\beta}_{TT}$ must be finite in order to measure this observable.

The matrix element form of the gluon transversity is,

$$\begin{aligned}-h_{1TT,g/B} = \Delta_T g(x) =& \varepsilon_{TT,\alpha\beta} \int \frac{d\xi^-}{2\pi} x p^+ e^{ixp^+\xi^-} \\ &\times \left\langle pE_x \left| A^\alpha(0) A^\beta(\xi) \right| pE_x \right\rangle_{\xi^+=\vec{\xi}_\perp=0}\end{aligned} \tag{38}$$

where $\epsilon_{TT}^{\alpha\beta} = +1$ for $\alpha = \beta = 1$, $\epsilon_{TT}^{\alpha\beta} = -1$ for $\alpha = \beta = 2$ and all else is zero. The linear polarization of the gluons requires a tensor polarized target oriented along the x-axis or the vertical direction transverse to the beam direction. This is indicated by the E_x in the above equation.

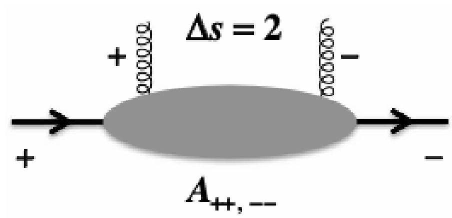

FIG. 9. Gluon-deuteron forward scattering amplitude $A_{++,--}$ with the spin flip of 2 ($\Delta s = 2$) for gluon transversity.

The cross section can be written in terms of parton correlation functions by considering the subprocess assuming a quark from the proton beam and an antiquark from the deuteron target ($q(p) + \bar{q}(d) \to \gamma + g$),

$$\begin{aligned} d\sigma_{pd\to\gamma X}|_{q\bar{q}\to\gamma^* g} =& \frac{1}{4p_A\cdot p_B} \int \frac{d^4p_a}{(2\pi)^4} \int \frac{d^4\gamma_b}{(2\pi)^4} \sum_{\text{spjin,favor}} \sum_{X_A,X_B} (2\pi)^4\delta^4\left(p_A - p_a - p_{AX}\right)(2\pi)^4\delta^4\left(p_B - p_b - p_{BX}\right) \\ & \times \left|\left\langle X_B\left|\bar{\psi}_{b,l}(0)\right| p_B s_B\right\rangle \left(\Gamma_{q\bar{q}\to\gamma^* g,\mu}\right)_{lk} \left\langle X_A\left|\psi_{a,k}(0)\right| p_A s_A\right\rangle M^{\mu}_{\gamma^*\to\mu^+\mu^-}\right|^2 \\ & \times \left(\frac{-e}{Q^2}\right)^2 (2\pi)^4\delta^4\left(p_a + p_b - k_1 - k_2 - p_d\right) \frac{d^3k_1}{2E_1(2\pi)^3}\frac{d^3k_2}{2E_2(2\pi)^3}\frac{d^3p_d}{2E_d(2\pi)^3} \end{aligned} \tag{39}$$

where the spin summations are over the muons, quark, antiquark, and gluon. The parton-interaction part is $\Gamma_{q\bar{q}} \to \gamma^* g, \mu = e_q \epsilon^{*\alpha}(p_d, \lambda_b)\Gamma_{\mu\alpha}$ by extraction of the quark charge e_q and the gluon-polarization vector $\epsilon^{*\alpha}(p_d, \lambda_d)$ from $\Gamma_{q\bar{q}\to\gamma^* g,\mu}$. By changing from three to two-body phase space and recalculating the cross section using the lepton and

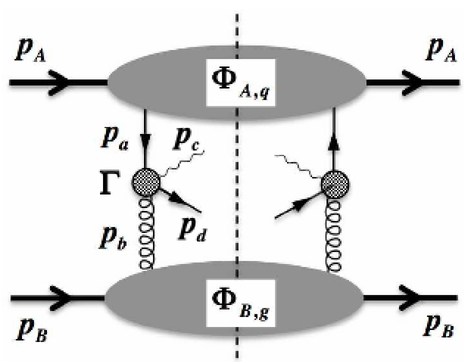

FIG. 10. The Quark-gluon process contribution to the cross section.

hadron tensor we get,

$$\frac{d\sigma_{pd\to\mu^+\mu^- X}}{d\tau dq_T^2 d\phi dy} = \frac{\alpha^2}{3(2\pi)^2 Q^4}\left(\int d\Phi_2\left(q; k_1, k_2\right) 2L^{\mu\nu}\right) W_{\mu\nu}, \tag{40}$$

where the hadron tensor for the $q\bar{q} \to \gamma^* g$ is,

$$\begin{aligned} W_{\mu\nu}(q\bar{q}) =& \int \frac{d^4p_a}{(2\pi)^4} \int \frac{d^4p_b}{(2\pi)^4} \sum_{\text{spin}_{c0lbr}} \sum_{q} \sum_{X_A,X_B} e_q^2 (2\pi)^4\delta^4\left(p_A - p_a - p_{AX}\right)(2\pi)^4\delta^4\left(p_B - p_b - p_{BX}\right) \\ & \times \left[\left\langle X_B\left|\bar{\psi}_{b,j}(0)\right| p_B s_B\right\rangle \left(\Gamma_{q\bar{q}\to\gamma' g,\mu}\right)_{ji} \left\langle X_A\left|\psi_{a,i}(0)\right| p_A s_A\right\rangle\right]^\dagger \left[\left\langle X_B\left|\bar{\psi}_{b,l}(0)\right| p_B s_B\right\rangle \left(\Gamma_{q\bar{q}\to\gamma^* g,\nu}\right)_{lk} \left\langle X_A\left|\psi_{a,k}(0)\right| p_A s_A\right\rangle\right] \\ & \times (2\pi)^4\delta^4\left(p_a + p_b - q - p_d\right)\frac{d^3p_d}{2E_d(2\pi)^3} \end{aligned} \tag{41}$$

Here the hadron tensor can be expressed in terms of the correlation functions. The quark-gluon process contribution to the cross section diagram is shown in Fig. 10 indicating the quark in the proton beam A and the gluon in the deuteron target B. The δ function $^4(p_H - p_h - p_{Hx})$ ($H = A$ or B, $h = a$ or b) are expressed by the integrals of exponential function: $(2\pi)^4\delta^4(p_H - p_h - p_{Hx}) = \int d^4\xi_h e^{-i(p_H - p_h - p_{H_x})\dot{\xi}_h}$. The quark field is given at ξ_h in the matrix elements with the exponential factor $e^{-i(p_H)\dot{\xi}_h}\psi(0)e^{-i(p_H)\dot{\xi}_h} = \psi(\xi_h)$.

III. THE MEASUREMENT

To measure transversity of both the sea-quarks and gluons in a polarized deuteron a set of unique target spin asymmetries must be measured. For the sea-quark transversity ideally what is needed is a transversely vector polarized target system which mitigates any tensor polarized contributions.

The gluon transversity is ideally measured with a vector and tensor polarized target as to isolate linearly polarized gluons in the deuteron. To understand this configuration we start again with the spin vector ($\boldsymbol{S}$) and tensor ($\boldsymbol{T}$) which are parameterized in the rest frame of the deuteron,

$$\boldsymbol{S} = (S_T^x, S_T^y, S_L) \tag{42}$$

$$\boldsymbol{T} = \frac{1}{2}\begin{pmatrix} -\frac{2}{3}S_{LL} + S_{\mathrm{TT}}^{xx} & S_{\mathrm{TT}}^{xy} & S_{LT}^{x} \\ S_{\mathrm{TT}}^{xy} & -\frac{2}{3}S_{LL} - S_{\mathrm{TT}}^{xx} & S_{LT}^{y} \\ S_{LT}^{x} & S_{LT}^{y} & \frac{4}{3}S_{LL} \end{pmatrix} \tag{43}$$

where S_T^x, S_T^y, S_{TT}^{xx}, S_{LT}^{xy}, and S_{LT}^y are the parameters to indicate the deuteron's vector and tensor polarizations. The deuteron polarization vector E is,

$$\begin{aligned} \vec{E}_0 &= (0,0,1) \\ \vec{E}_\pm &= \tfrac{1}{\sqrt{2}}(\mp 1, -i, 0) \\ \vec{E}_x &= \tfrac{1}{\sqrt{2}}\left(\vec{E}_- - \vec{E}_+\right) = (1,0,0) \\ \vec{E}_y &= \tfrac{i}{\sqrt{2}}\left(\vec{E}_- + \vec{E}_+\right) = (0,1,0) \end{aligned} \tag{44}$$

where E_+, E_0 and E_- indicate the three possible spin states of the deuteron. Here the polarizations E_x and E_y are spin-1 alignment dependent states and can be used to orient the gluons in a linearly polarized configuration in the target based on the gluon transversity distributions defined by the matrix elements between linearly-polarized states. The spin vector and tensor are written in terms of the polarization vector E of the deuteron as,

$$\vec{S} = \mathrm{Im}\left(\vec{E}^* \times \vec{E}\right), \quad T_{ij} = \frac{1}{3}\delta_{ij} - \mathrm{Re}\left(E_i^* E_j\right). \tag{45}$$

For best gluon transversity extraction the key to an optimized target configuration is to selectively reduce all unneeded terms in the spin tensor to zero preserving only the terms that relate to the observable of interest. In this case having a finite S_{TT}^{xx} gives the desired access to the gluon transversity. Making the other terms zero or negligible is advantageous to a clean measurement. In this case the polarization vectors E_x and E_y can be used to provide linear polarization and both consist of a deuteron tensor polarized in the transverse plane to the beam-line. The difference in the cross section from these polarization states can be used in an asymmetry to build an observable to extract gluon transversity.

The polarization vectors E_x, E_0 E_y are all indicative of a purely tensor polarized target with spin quantization axis along the x, z, and y axis respectively. From Eq. 45 we get for E_x a vector polarization of $S_T^x = S_T^x = S_T^x = S_T^x = 0$, with $S_{LL} = 1/2$, $S_T^{xx} = -1$, and $S_{TT}^{xy} = S_{LT}^x = S_{LT}^y = 0$. For E_y a vector polarization of $S_T^x = S_T^x = S_T^x = S_T^x = 0$, with $S_{LL} = 1/2$, $S_T^{xx} = +1$, and $S_{TT}^{xy} = S_{LT}^x = S_{LT}^y = 0$ is obtained. For E_0 a vector polarization of $S_T^x = S_T^x = S_T^x = S_T^x = 0$, with $S_{LL} = -1$, $S_T^{xx} = 0$, and $S_{TT}^{xy} = S_{LT}^x = S_{LT}^y = 0$ is obtained. We can then use combinations to optimize such that $E_x - E_y$ yields $S_T^x = S_T^x = S_T^x = S_T^x = 0$, with $S_{LL} = 0$, $S_T^{xx} = -2$ and $S_{TT}^{xy} = S_{LT}^x = S_{LT}^y = 0$. Also $2E_x - E_0$ yields $S_T^x = S_T^x = S_T^x = S_T^x = 0$, with $S_{LL} = 0$, $S_T^{xx} = -2$, and $S_{TT}^{xy} = S_{LT}^x = S_{LT}^y = 0$. With either of these configurations the longitudinal tensor polarization is zero as well as any vector polarization contributions and the critical term S_{TT}^{xx} is also maximized.

To exploit the observables we rely on the correlation functions in the collinear formalism. For the difference in the E_x and E_y polarized cross section the hadron tensor is given by,

$$W_{\mu\nu}\left(E_x - E_y\right) = \sum_{\lambda_d}\sum_{\mathrm{color}}\sum_q e_q^2 \int_{\min(x_a)}^1 dx_a \frac{\pi}{p_g^-\left(x_a - x_1\right)} \mathrm{Tr}\left[\Gamma_{\nu\beta}\left\{\Phi_{q/A}\left(x_a\right) + \Phi_{\bar{q}/A}\left(x_a\right)\right\}\hat{\Gamma}_{\mu\alpha}\Phi_{g/B}^{\alpha\beta}\left(x_b\right)\right]. \tag{46}$$

Here the summation is taken over the quark spin λ_d and all spin tensor matrix elements are zero except for the gluon transversity in the target. There is no equivalent polarization term in the quark and antiquark distributions of the spin-1 target so the transversity of the sea-quarks and the gluons can be separated through the strategic use of vector and tensor polarizations. This is because the virtual photon in the intermediate stage interacts with a charge parton so only quark and antiquark correlation functions contribute as the leading process from the spin-1/2 nucleons inside the spin-1 deuteron. This implies that the geometric shape the deuteron in the different M_J spin states are highly correlated to the transverse gluon and sea-quark observables.

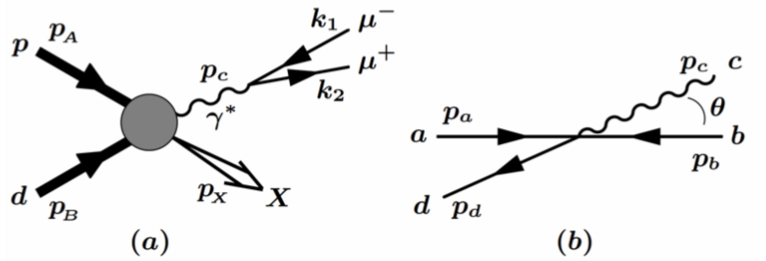

FIG. 11. (a) The proton-deuteron Drell-Yan process $p + d \to \mu^+\mu^- + X$ showing the notation for each momentum index. (b) The parton reaction with corresponding index for process $a + b \to c + d$ in the center-of-momentum frame.

To build an asymmetry the cross section difference is written as,

$$\begin{aligned}\frac{d\sigma_{pd\to\mu^+\mu^-X}}{d\tau dq_T^2 d\phi dy}\left(E_x - E_y\right) = &-\frac{\alpha^2\alpha_s C_F q_T^2}{6\pi s^3}\cos(2\phi)\int_{\min(x_a)}^1 dx_a \frac{1}{\left(x_a x_b\right)^2\left(x_a - x_1\right)\left(\tau - x_a x_2\right)^2} \\ &\times \sum_q e_q^2 x_a\left[q_A\left(x_a\right) + \bar{q}_A\left(x_a\right)\right] x_b \Delta_T g_B\left(x_b\right).\end{aligned} \tag{47}$$

The cross section sum of these polarization states can also be calculated where $\bar{q}q \to \gamma^* g$ and $q/\bar{q} \to \gamma^* q/\bar{q}$. Leading to the cross section,

$$\begin{aligned}\frac{d\sigma_{pd\to\mu^+\mu^-X}}{d\tau dq_T^2 d\phi dy}\left(E_x + E_y\right) = &\frac{\alpha^2\alpha_s C_F}{2\pi\tau s^2}\int_{\min(x_a)}^1 dx_a \frac{1}{\left(x_a - x_1\right) x_a^2 x_b^2} \\ &\times \sum_q e_q^2 \left[\frac{4}{9}\left\{q_A\left(x_a\right)\bar{q}_B\left(x_b\right) + \bar{q}_A\left(x_a\right) q_B\left(x_b\right)\right\}\right. \\ &\times \frac{2\tau\left\{\tau - \left(-2x_a x_b + x_1 x_b + x_2 x_a\right)\right\} + x_b^2\left(x_a - x_1\right)^2 + x_a^2\left(x_b - x_2\right)^2}{\left(x_a - x_1\right)\left(x_b - x_2\right)} \\ &+ \frac{1}{6}\left\{q_A\left(x_a\right) + \bar{q}_A\left(x_a\right)\right\} g_B\left(x_b\right)\frac{2\tau\left(\tau - x_1 x_b\right) + x_b^2\left\{\left(x_a - x_1\right)^2 + x_a^2\right\}}{x_b\left(x_a - x_1\right)} \\ &\left. + \frac{1}{6} g_A\left(x_a\right)\left\{q_B\left(x_b\right) + \bar{q}_B\left(x_b\right)\right\}\frac{2\tau\left(\tau - x_2 x_a\right) + x_a^2\left\{\left(x_b - x_2\right)^2 + x_b^2\right\}}{x_a\left(x_b - x_2\right)}\right]\end{aligned} \tag{48}$$

This provides the necessary numerator to construct a gluon transversity asymmetry which can be written as,

$$A_{E_{xy}} = \frac{d\sigma_{pd\to\mu^+\mu^-X}\left(E_x - E_y\right)/\left(d\tau dq_T^2 d\phi dy\right)}{d\sigma_{pd\to\mu^+\mu^-X}\left(E_x + E_y\right)/\left(d\tau dq_T^2 d\phi dy\right)}. \tag{49}$$

Based on the polarization vector difference an equivalency can be derived using the unpolarized combination vector $E_x + E_y + E_z := U$, resulting is zeros for all terms in the spin polarization vector and tensor. We can then write $E_x - E_y \equiv 2E_x + E_0 - U$ and $E_x + E_y \equiv U - E_0$. If we assume that the differential cross section from longitudinal tensor polarization is small compared to the transverse tensor polarization when the quantization axis of the target is pointing in the transverse direction then we can write,

$$A_{E_{xy}} = \frac{d\sigma_{pd\to\mu^+\mu^-X}\left(E_x - E_y\right)/\left(d\tau dq_T^2 d\phi dy\right)}{d\sigma_{pd\to\mu^+\mu^-X}\left(E_x + E_y\right)/\left(d\tau dq_T^2 d\phi dy\right)} = \frac{d\sigma_{pd\to\mu^+\mu^-X}\left(2E_x - U\right)/\left(d\tau dq_T^2 d\phi dy\right)}{d\sigma_{pd\to\mu^+\mu^-X}\, U/\left(d\tau dq_T^2 d\phi dy\right).}$$

The generalized experimental gluon transversity asymmetry can then be written as,

$$A_{E_{xy}} = \frac{1}{fP_{zz}}\frac{2\sigma_{pd\to\mu^+\mu^-X}^{E_x} - \sigma_{pd\to\mu^+\mu^-X}^{U}}{\sigma_{pd\to\mu^+\mu^-X}^{U}}, \tag{50}$$

where P_{zz} is the target ensemble tensor polarization and f is the correction for the presence of unpolarized nuclei the beam interacts with. There are several ways to build a gluon transversity asymmetry using different quantization axes and polarized target configuration, but this equivalence provides as way to compare directly with predictions and requires the same polarized target magnet and orientation already in place in the SpinQuest experimental hall. Also due to the cos2ϕ term in Eq. 47 it is possible to extract a tensor polarization contribution in the azimuthal angle produced by gluon transversity. This would show up even from the E_x polarized state alone and the difference between a target with some tensor polarization and with no-tensor polarization can be use to measure the whole coefficient while exploring any azimuthal dependence.

As mentioned previously the quark transversity is easiest to measure in the neutron/deuteron by mitigating any contribution from the tensor polarization. The best possible target system would then alternate between vector polarized, tensor polarized and unpolarized. With the UVA RF technology it is possible to start with a target that is in Boltzmann equilibrium which has both tensor and vector polarization, then on the scale of milliseconds, use the selective RF in the NMR frequency domain to remove tensor polarization in the target ensemble, as well as to create a unpolarized target and then flip back to the original spin state. These alterations to the target spin configurations can be done between beam spills allowing data collection in the different spin states while minimizing time dependant false asymmetries.

As mentioned the SpinQuest polarized target system can already accommodate most of the needs of this proposal. Only slight modification must be made to the target cell to add the selective RF manipulation coil and adapt the polarization measuring NMR system to be optimized to function with the two competing RF sources. For the purpose of the proposed measurements, one needs to separately measure different target spin configurations but with the field always pointing transverse vertical as it is now. The experimental setup and data taking approach we will follow is similar to that used previously by experiments E866 and E906 to measure the $\bar{d}$ /$\bar{u}$ ratio in the proton. A transversely polarized deuteron target is used as for the $\bar{d}$ Sivers measurement for part of E1039, with the neutron providing additional $\bar{d}$ (sea) quarks that annihilate with valence d quarks from the beam.

Target material ND_3 can be used to provide the transversely polarized neutron target. Here the dilution factor is higher (0.3) than that of the proton, with a maximum vector polarization of up to 50% with a tensor polarization of 20% under Boltzmann equilibrium. This target can be RF manipulated to have a tensor polarization of over 35% or 0%. The ND_3 target materiel is highly radiation resistant and has been a go to target for decades yet there are still new target systems being developed to leverages its full potential. The DN_3 is our source for tensor observables as the spin-1 system but also our source for neutron vector polarized observables. The neutron polarization is always 91% of the vector polarization of the deuteron.

IV. EXPERIMENTAL SETUP

A. The Spectrometer

We are proposing to use the existing SpinQuest/SeaQuest [105] Fig.12 spectrometer to perform our measurement. The spectrometer consists of two magnets, FMAG and KMAG ,and four tracking stations, where the last one serves as a muon identifier. The first magnet (FMAG) is now almost entirely surrounded in shielding blocks for use in SpinQuest and future experiments. This magnet is a closed-aperture, solid iron magnet. The beam protons that do not interact in the targets are absorbed in the iron of the first magnet, which allows only muons to traverse the remaining spectrometer. The downstream magnet (KMag) is a large, open-aperture magnet that was previously used in the Fermilab KTeV experiment. Each of the tracking/triggering stations consists of a set of scintillator hodoscopes to provide fast signals for the FPGA-based trigger system and a drift chambers.

Muon identification is accomplished with station 4, which is located downstream of a 1 m thick iron wall. Like the other stations, this station contains both triggering hodoscopes and tracking detectors. The station 4 tracking detectors consist of 4 layers of proportional tube planes. Each plane is made of 9 proportional tube modules, with each module assembled from 16 proportional tubes, each 3.66 m long with a 5.08 cm diameter, staggered to form two sub-layers.

This spectrometer was designed to perform Drell-Yan measurements at large x_1 . This is illustrated in Fig. 13, where the acceptance of the SpinQuest detector is plotted as function of x_1 (x-axis) and x_2 (y-axis).

This is an excellent kinematic range for the proposed sea quark and gluon transversity measurements, covering the region of large anti-down quark excess observed by E866, where large pion-cloud effects may be expected. The contributions from target valence quarks at large x_2 are then negligible.

The experiment will be using the Fermilab main injector beam with an energy of 120 GeV and a 4.4 second spill every minute. The maximum beam intensity will be 3×10^{12} protons per spill which is defined by the polarized target and spectrometer.

B. SpinQuest Construction Status

The SpinQuest shielding assessment is complete and approved and the construction is complete except for the remaining roof on the cave. The polarized target system is in place and the cryogenic safety review has been completed and has passed.

The helium liquification system and roots pumps for the high power evaporation refrigerator has been installed and is ready for testing.

The beam line and collimator have also been installed and approved. Fig. 14 shows the target system and shielding cave with the spectrometer down stream to run SpinQuest. The upstream perspective is shown in Fig. 15.

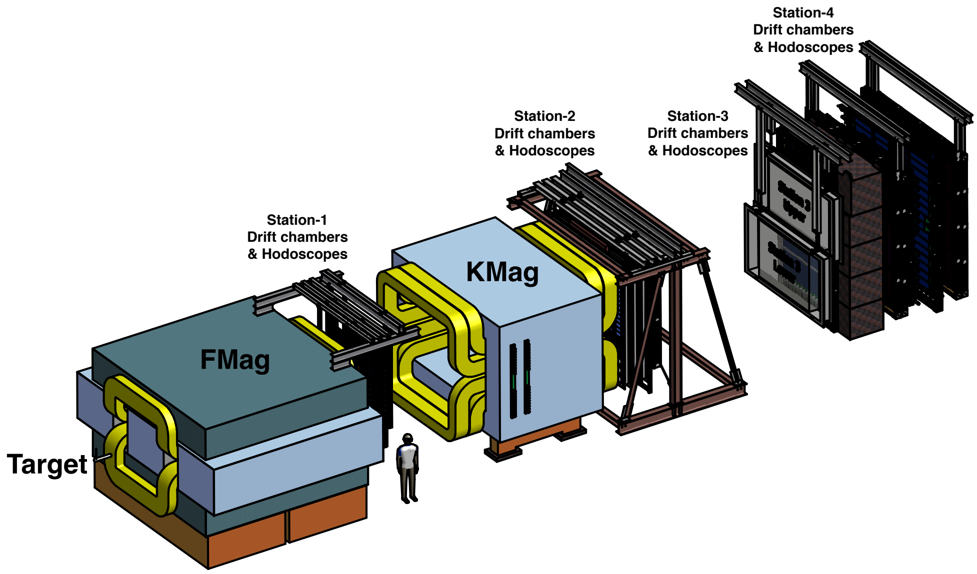

FIG. 12. The SeaQuest Spectrometer

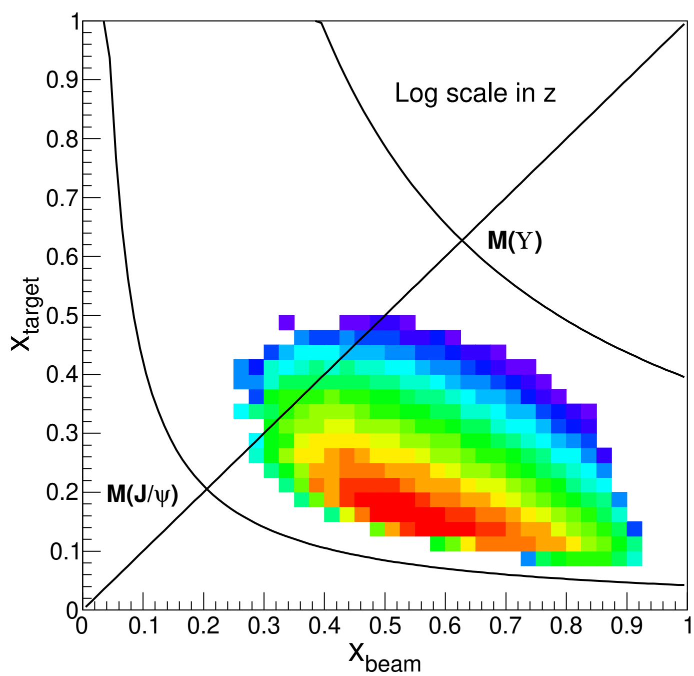

FIG. 13. The acceptance of SeaQuest Spectrometer with polarized target.

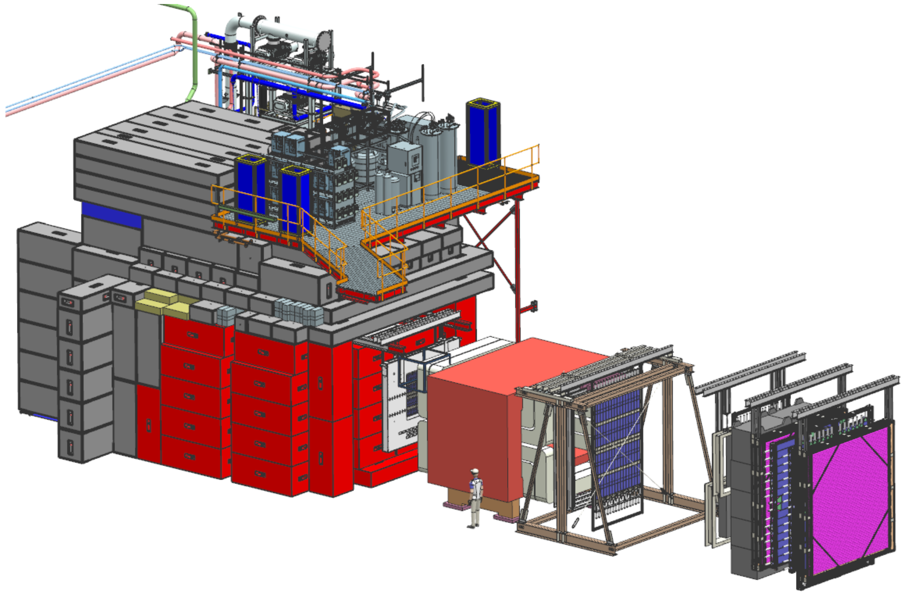

FIG. 14. The target Cave and spectrometer down stream. The red shielding blocks are surrounding FMag. The new UVA helium liquifier is setup on top of the new cryo-platform. Image courtesy of Don Mitchell of Fermilab.

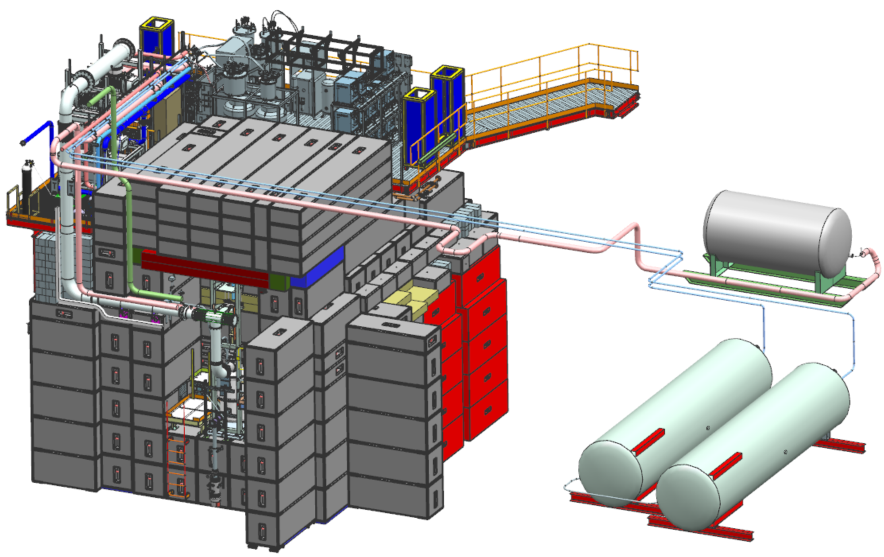

FIG. 15. The target cave show from the upstream end with the SpinQuest target system shown in place. The connecting storage tanks for Helium gas and liquid nitrogen are out side of the NM4 building.

C. The Polarized Target

The proposal requires the same SpinQuest polarized target which has been rebuilt and tested at UVA and recently installed in the NM4 experimental hall at Fermilab. The target system consists of a 5T superconducting split coil magnet, a ^{4}He evaporation refrigerator, a 140 GHz microwave source and a large 15000 m^3/hr pumping system. The target is polarized using Dynamic Nuclear Polarization (DNP) [106] and is shown schematically in Fig. 16. In the left hand picture the target cave entrance is shown and the polarized target with beam line connection from the upstream perspective can be seen. In the right hand picture the cross sectional drawing of the polarized target showing the target insert, the evaporation refrigerator, and the superconducting magnet. The beam direction is from right to left, and the field direction is vertical along the symmetry axis, so that the target polarization is transverse to the beam direction. The UVA refrigerator is also shown with the target insert holding the polarized target material (ND_3) with the top cell in the center of the split coils.

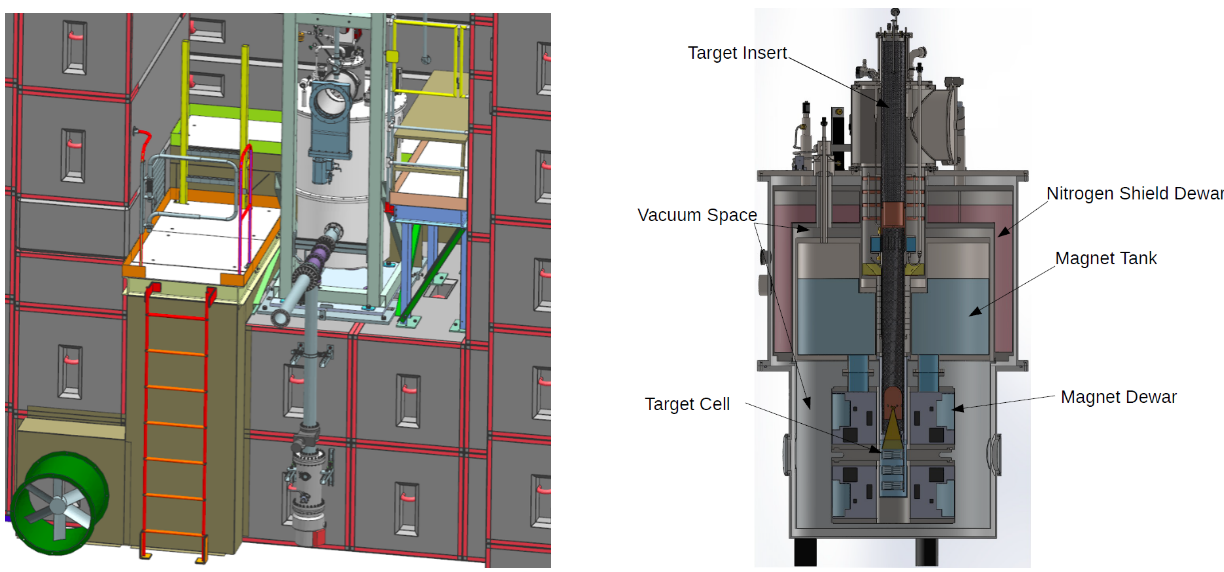

FIG. 16. *(Left) The target cave entrance and the polarized target with beam line connection from the upstream perspective. (Right) Cross sectional drawing of the polarized target showing the target insert, the evaporation refrigerator, and the superconducting magnet.*

While the magnetic moment of the proton is too small to lead to a sizable polarization in a 5 T field through the Zeeman effect, electrons in that field at 1 K are better than 99% polarized. By doping a suitable solid target material with paramagnetic radicals to provide unpaired electron spins, one can make use of the highly polarized state of the electrons. The dipole-dipole interaction between the nucleon and the electron leads to hyperfine splitting, providing the coupling between the two spin species. By applying a suitable microwave signal, one can populate the desired spin states. As mentioned, we will use frozen ammonia beads [107] of and ND_3 as the target material and create the paramagnetic radicals (roughly 10^{19} spins/ml) through irradiation with a high intensity electron beam at NIST. The cryogenic refrigerator, which works on the principle of liquid ^{4}He evaporation, can cool the bath to 1 K, by lowering the ^{4}He vapor pressure down to less than 0.118 Torr. The polarization will be measured with NMR techniques with three NMR coils per cell, placed inside each target cell. The maximum polarization achieved with the deuteron target is around 50% vector polarization and the ammonia bead packing fraction is about 60%. In our estimate for the statistical precision, we have assumed an average polarization of 32% vector polarization. The polarization dilution factor, which is the ratio of free polarized deuterons to the total number of nucleons, is 3/10 for ND_3, due to the presence of nitrogen. The target material will need to be replaced approximately every 8-10 days in all three target cells, due to the beam induced radiation damage. This work will involve replacing the target material in the target insert, cooling down the target and performing multiple thermal equilibrium measurements. From previous experience, we estimate that this will take about a shift to accomplish. Careful planning of these changes will reduce the impact on the beam time. Furthermore, we will be running with three active targets on one target insert, thus reducing any additional loss of beam time. The target cells are about 80 mm long and hold about 12 grams of ND_3. Each cell contains 3 NMR coils spaced evenly over the whole length.

Polarization of spin-1 deuterons can be achieved using DNP with deuterated materials like ND_3, C_4D_9OH or LiD. In the spin-1 targets the deuterons have nonzero quadrupole moments, and the structural arrangement of the nuclei in the solid generate electric field gradients (EFG) which couple to the quadrupole moment. This results in an additional degree of freedom in polarization that the spin-1/2 nucleons do not possess. The target spins in the ensemble can be aligned in both a vector (P) and tensor (P_{zz}) polarization. Defined in terms of the relative occupation of the three magnetic substates of the spin-1 system ($m = 0, \pm 1$) they are,

$$P = \frac{n_+ - n_-}{N}$$

and

$$P_{zz} = \frac{n_+ - 2n_0 + n_-}{N},$$

with n_i being the relative occupation of the magnetic substate with $m = i$, and $N = n_+ + n_0 + n_-$.

1. NMR Measurements

The proton spin polarization is measured with a continuous-wave NMR system based on the Liverpool Q-meter design [?] and recently upgraded at LANL. The Q-meter works as part of a circuit with phase sensitivity designed to respond to the change of the impedance in the NMR coil. The radio-frequent (RF) susceptibility of the material is inductively coupled to the NMR coil which is part of a series LCR circuit, tuned to the Larmor frequency of the nuclei being probed. The output, consisting of a DC level digitized and recorded as a target event [106] in the target data acquisition system.

The polarized target NMR and data acquisition included the software control system, the Rohde & Schwarz RF generator (R&S), the Q-meter enclosure, and the target cavity insert. The Q-meter enclosure contains a series of Q-meters circuits with separate connection cables which are used for different target cup cells during the experiment. The target material and NMR coil are held in polychlorotrifluorethylene (Kel-F) cells with the whole target insert cryogenically cooled to 1 K. Kel-F is used because it contains no free protons.

The R&S generator produces a RF signal which is frequency modulated to sweep over the frequency range of interest. Typically, the R&S responds to an external modulation, sweeping linearly from 400 kHz below to 400 kHz above the Larmor frequency. The signal from the R&S is connected to the NMR coils within the target material. To avoid degrading reflections in the long connection from the NMR coil to the electronics, a standing wave can be created in the transmission cable by selecting a length of cable that is an integer multiple of the half-wavelength of the resonant frequency. This specialized connection cable is known as the $\lambda/2$ cable and is a semi-rigid cable with a teflon based dielectric. The NMR coil a set of loops made of 70/30 copper-nickel tube, which minimizes interaction with the proton beam. The coil opens up into an oval shape spanning approximately 2 cm inside the cup. It is possible to enhance signal to noise information through the software control system by making multiple frequency sweeps and averaging the signals. A completion of the set number of sweeps results in a single target event with a time stamp. The averaged signal is integrated to obtain a NMR polarization area for that event. Each target event written contains all NMR system parameters and the target environment variables needed to calculate the final polarization. The on-line target data and conditions are analyzed over the experiments set of target events to return a final polarization and associated uncertainty for each run.

A target NMR calibration measurement or Thermal Equilibrium measurement (TE) is used to find a proportionality relation to determine the enhanced polarization under a range of thermal conditions given the area of the "Q-curve" NMR signal at the same magnetic field. The magnetic moment in the external field results in a set of $2J+1$ energy sublevels through Zeeman interaction, where J is the particle spin. The TE natural polarization for a spin-1/2 particle is given by,

$$P_{TE} = \tanh\left(\frac{\mu B}{kT}\right), \tag{51}$$

coming from Curie's Law [?], where μ is the magnetic moment in the external field of strength B, k is the Boltzmann constant, and T the temperature. Measuring P_{TE} at low temperature increases stability and the polarization signal. This is favorable being that the uncertainty in the NMR signal increases as the area of the signal decreases. In fact much of the target uncertainty comes from error in the calibration. The goal temperature used is $\sim$1.4 K.

The dynamic polarization value is derived by comparing the enhanced signal S_E integrated over the driving frequency ω, with that of the (TE) signal:

$$P_E = G\frac{\int S_E(\omega)d\omega}{\int S_{TE}(\omega)d\omega}P_{TE} = GC_{TE}A_E, \tag{52}$$

and calibration constant defined as,

$$C_{TE} = \frac{P_{TE}}{A_{TE}}. \tag{53}$$

Where P_E (A_E) is the polarization (area) of the enhanced signal and P_{TE} (A_{TE}) is the polarization (area) from the thermal equilibrium measurement. The uncertainty in the calibration constant, $\delta C_{TE}/C_{TE}$, can easily be calculated using the fractional error from P_{TE} and A_{TE}. The ratio of gains from the Yale card used during the thermal equilibrium measurement to the enhanced signal is represented as G. For more detail see, [110].

2. Neutron Polarization Measurements

The deuteron polarization will be monitored by the same LANL continuous wave NMR system as used for the proton with one small change. There are two means whereby the polarization can be extracted from the NMR signal: the area method and the peak-height method. We intend to use both.

First, the total area of the NMR absorption signal is proportional to the vector polarization of the sample, and the constant of proportionality can be calibrated against the polarization of the sample measured under thermal equilibrium (TE) conditions. This is the standard method used for polarized proton targets, but can be more problematic for deuteron targets. Typical conditions for the TE measurements are 5 T and 1.4 K, where the deuteron polarization is only 0.075%, compared to 0.36% for protons. This smaller polarization, along with quadrupolar broadening, makes the deuteron TE signal more difficult to measure with high accuracy. A cold NMR system can be used to improve the signal-to-noise ratio of the NMR signal [111].

The deuteron polarization can also be extracted from the shape of the NMR signal. The deuteron is a spin-1 nucleus with three magnetic substates, $m = -1, 0, +1$, and the NMR absorption signal lineshape is the sum of the two overlapping absorption lines consisting of the $-1 \to 0$ and $0 \to +1$ transitions. In the case of $^{14}ND_3$, the deuteron's electric quadrupole moment interacts with electric field gradients within the molecule and splits the degeneracy of the two transitions. The degree of splitting depends on the angle between the magnetic field and direction of the electric field gradient. The resultant linshape, integrated over a sample of many polycrystalline beads has the form of a Pake doublet [113]. has been experimentally demonstrated that, at or near steady-state conditions, the magnetic substates of deuterons in dynamically polarized $^{14}ND_3$ are populated according to the Boltzmann distribution with a characteristic spin temperature T that can be either positive or negative, depending on the sign of the polarization.

When the system is at thermal equilibrium with the solid lattice, the deuteron polarization is known from:

$$P_z = \frac{4 + \tanh \frac{\mu B}{2kT}}{3 + \tanh^2 \frac{\mu B}{2kT}} \tag{54}$$

where μ is the magnetic moment, and k is Boltzmann's constant. The vector polarization can be determined by comparing the enhanced signal with that of the TE signal (which has known polarization). This polarimetry method is typically reliable to about 5% relative.

Similarly, the tensor polarization is given by:

$$P_{zz} = \frac{4 + \tanh^2 \frac{\mu B}{2kT}}{3 + \tanh^2 \frac{\mu B}{2kT}} \tag{55}$$

From Eqs. 54 and 55, we find:

$$P_{zz} = 2 - \sqrt{4 - 3P_z^2} \tag{56}$$

In addition to the TE method, polarizations can be determined by analyzing NMR lineshapes as described in [**?**] with a typical 5-7% relative uncertainty. At high polarizations, the intensities of the two transitions differ, and the NMR signal shows an asymmetry R in the value of the two peaks. The vector polarization is then given by:

$$P_z = \frac{R^2 - 1}{R^2 + R + 1} \tag{57}$$

and the tensor polarization is given by:

$$P_{zz} = \frac{R^2 - 2R + 1}{R^2 + R + 1} \tag{58}$$

This measuring technique can be used as a compliment to the TE method resulting in reduced uncertainty in polarization for vector polarizations over 28%.

The measurement of the neutron polarization (P_n) is achieved by a calculation using the NMR measured polarization of the deuteron (P_d). The quantum mechanical calculation using Clebsch-Gordan coefficients show 75% of the neutron spins in the D-state are antiparallel to the deuteron spins. The resulting neutron polarization is,

$$P_n = (1 - 1.5\alpha_D)P_d \approx 0.91P_d,$$

where α_D is the probability of the deuteron to be in a D-state.

3. *The Deuteron NMR Lineshape*

The quadrupole moment of the spin-1 nuclei results from the nonspherically symmetric charge distribution in the quadrupolar nucleus. For materials without cubic symmetry (e.g. C_4D_9OH or ND_3), the interaction of the quadrupole moment with the EFG breaks the degeneracy of the energy transitions, leading to two overlapping absorption lines in the NMR spectra. The spin-1 NMR lineshape is shown in Fig. 17 demonstrating the two intensities I_+ (in blue) and I_- (in red). In terms of population,

$$I_+ = C(\rho_+ - \rho_0)$$

and

$$I_- = C(\rho_0 - \rho_-),$$

where ρ_x is the population density in the $m = x$ energy level and C is the calibration constant. The term intensity is used here to indicate both the height and area of these two individual regions. The frequency is indicated by a dimensionless position in the NMR line $R = (\omega - \omega_D)/3\omega_Q$ which spans the domain of the NMR signal, where ω_Q is the quadrupolar coupling constant. In these units $R = 0$ corresponds to the Larmor frequency of the deuteron at 5 T ($\omega_D = 32.679$ MHz). The local electric field gradients that couple to the quadrupole moments of the spin-1 system causing an asymmetric splitting of the energy levels into two overlapping absorption lines. The energy levels of the non-cubic symmetry spin-1 system can be expressed as,

$$E_m = -\hbar\omega_D m + \hbar\omega_Q(3\cos^2\theta - 1 + \eta\sin^2\theta\cos2\phi)(3m^2 - 2),$$

where θ is the polar angle between the axis of the deuteron bond and the magnetic field, see Fig. 18. The azimuthal angle ϕ and parameter η are fixed parameters used to characterize the electric field gradient with respects to the deuteron bond axis. The degree of axial symmetry and dependence on the polar angle can be understood from the basis lineshape for an isotropic rigid

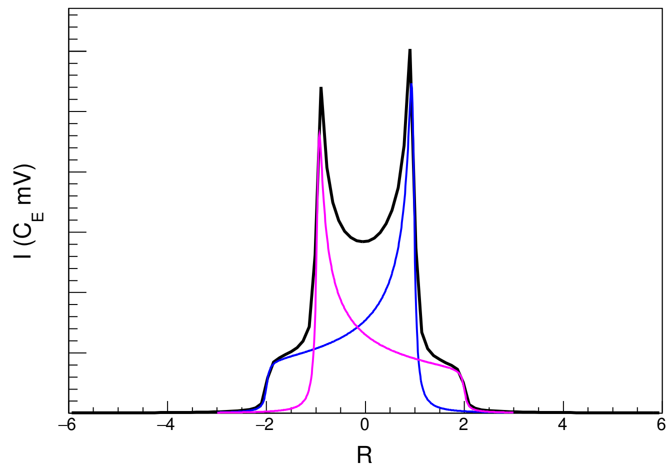

FIG. 17. An example of the NMR lineshape of a spin-1 target with a non-cubic symmetry demonstrating the two overlapping absorption lines. The two intensities of the signal I_+ and I_- are shown in blue and pink respectively. Figure from [112].

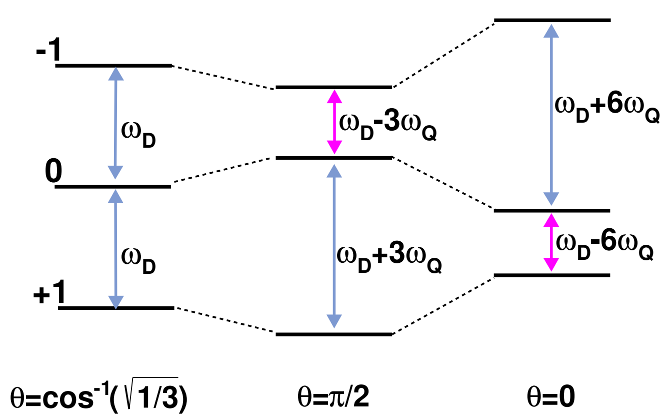

FIG. 18. The energy level diagram for deuterons in a magnetic field for three values of θ where $\hbar\omega_D$ is the deuteron Zeeman energy, $\hbar\omega_Q$ is the quadrupole energy. The color indicates which transition corresponds to which peak shown in Fig. 17. Figure from [112].

solid which is known as a Pake doublet. The polarization information can be extracted from a fit of the NMR data providing the areas of the two intensities [114, 115]. The peaks of the Pake doublet ($R \sim \pm 1$) correspond to the principal axis of the coupling interaction being perpendicular ($\theta = \pi/2$) to the magnetic field. This is the most probable configuration within each transition, as indicated by the height in the intensity of each peak. The opposing end in each absorption line, called the pedestal, corresponds to the configuration when the principal axis of the coupling interaction is parallel ($\theta = 0$) to the magnetic field, which has much less statistical significance as indicated by the small relative height in the intensities in each transition around ($R \sim \mp 2$).

If the ensemble of the spin system is in thermodynamic equilibrium the ratio of the intensities ($r = I_+/I_-$) can be used to extract the polarizations directly [114].

$$P = \frac{r^2 - 1}{r^2 + r + 1} \qquad P_{zz} = \frac{r^2 - 2r + 1}{r^2 + r + 1} \tag{59}$$

or simply,

$$\frac{P_{zz}}{P} = \frac{r - 1}{r + 1}. \tag{60}$$

The extracted information from the fit also gives the sum of the two intensities which provides the vector polarization $P = C(I_+ + I_-)$ while the difference provides the tensor polarization $P_{zz} = C(I_+ - I_-)$. It is important to note that these two expressions remain true even if the system is not in thermodynamic equilibrium unlike Eq. 59 and 60. Once the calibration constant C is measured, these expressions can be used to extract the averaged polarizations of the ensemble over the course of the HEP/Nuclear scattering experiment [110].

4. Tensor Polarization Enhancement

To manipulate the magnitude of tensor polarization during DNP pumping a separate source of coil generated RF irradiation is used to selectively saturate some portion of the deuteron NMR line. By applying RF irradiation at a frequency or over a frequency range (hole burning [116, 117]), transitions are induced between the magnetic sublevels within the frequency domain of the applied RF. A spin-diffusion rate that is small compared to the effective nuclear relaxation rate allows for significant changes to the NMR line via the RF, which can be strategically applied to manipulate the spin-1 tensor polarization. In the presented set of measurements DNP microwaves were used as well as an additional RF source that used semi-saturating RF (ss-RF) irradiation to maximize the tensor polarization for the 1 K and 5 T system [115]. A semi-saturated steady-state condition is used which manipulates and holds the magnetic sublevels responsible for polarization enhancement. The continuous wave NMR (CW-NMR) lineshape is measured and manipulated to maximize tensor polarization. The technique of ss-RF requires using a power profile that is sensitive to the intensity distributions with the correct modulation time signature over the frequency domain to optimally enhance. To be useful in a scattering experiment setting, the target ensemble averaged tensor polarization must be increased and held during the beam spill. Temporarily enhanced states during beam-target interactions are much more plausible at facilities that have a short beam spill per cycle such as Fermilab. This allows significant beam intensity on a target that is RF-manipulated for a short period, and then gives significant recovery time to build up polarization again for the next spills.

The source of ss-RF comes from a dedicated coil with a field $\mathbf{B}_\nu$ resulting in an induced transition rate proportional to [115],

$$\xi = 2\pi \frac{\mathbf{B}_\nu a_\nu}{\mathbf{B}_0} \delta(\omega_D - \omega_\nu), \tag{61}$$

where ω_D is the Larmor frequency, ω_ν is the ss-RF frequency and a_ν is the coupling constant and $\mathbf{B}_0$ is the strength of the holding field. The ss-RF can only play a role between nuclear spin energy levels that differ by the spin of the mediating photon. The ss-RF drives transitions that lead to equalization of the populations in the energy levels at the applied frequencies. This implies that the change in intensities at the location R in the NMR line due to the ss-RF can be expressed as,

$$\frac{I_\pm(R)}{dt} = -2\xi\omega_1 I_\pm(R), \tag{62}$$

$$\frac{I_\mp(-R)}{dt} = \xi\omega_1 I_\pm(R). \tag{63}$$

In other words the rate at which any one of the intensities change due to ss-RF is only dependent on the intensity level and the strength of the $\mathbf{B}_\nu$ field, or RF power. Here ω_1 is the reciprocal of the electron longitudinal relaxation rate used to be consistent with previous work [115]. The total polarization can only be decreased at the ss-RF location in R so strategic implementation is required to enhance the difference in the integrated I_+ and I_- regions. Equation 63 indicates that for any region at R in the intensity reduced by the ss-RF also results in the increase in the opposite signed intensity growing at $-R$ at half the rate as the decrease seen at R. This also implies that the region at $-R$ increases in area by half of the lost area at R.

Equations 62 and 63 affirms that materials with the same lineshape can be treated exactly the same under ss-RF tensor enhancement. This expression does not change for different materials relaxation rates. The nuclear spin polarization is measured with an CW-NMR system [108]. With this system the RF susceptibility of the material is inductively coupled to the NMR coil which is part of a series LCR Q-meter circuit that is tuned to the Larmor frequency of the nuclei of interest. The Q-meter based NMR provides a non-destructive polarization probe of the nuclear spin ensemble in the solid-state target.

For the selective excitation using ss-RF, an additional coil around the target cup is necessary. This additional RF coil is connected to an RF-generator and amplifier. The ss-RF coil consists multiple turns of silver covered copper clad non-magnetic steel with a diameter of ∼0.2 mm. The coil is constructed to approximate a homogeneous RF field around the target material that is perpendicular to the holding field. For optimal performance the coil is both impedance matched and tuned as an LCR circuit to maximize power and reduce reflection at the coil. The ss-RF is modulated over the frequency domain of interest at the appropriate RF power to semi-saturate the NMR line to the intensity level of interest. This same RF circuit can be used to perform an Adiabatic fast passage (AFP) on the target. A half AFP can be used to unpolarized the target putting 50% of the target polarization in the opposing direction. The RF sweep rate to achieve an AFP is on the order of a few milliseconds.

The distribution of the power profile delivered is also dependant on the coil. A high quality factor and optimized tune in the ss-RF coil delivers a more precise and localized RF load in the signal domain. The power profile of the ss-RF in the CW-NMR is characterized by the Voigt function [115].

The material of choice is ND_3 primarily because if has the desired lineshape and it is highly radiation resistant as well as offering the best polarization and dilution factor out of all possible polarized target materials. However because of its long relaxation rate ND_3 does take a while to fully polarized (several hours) and it will maximizes at only about 50%. This experiment would require tensor polarization as well which is calculated from the equilibrium relation between the energy level. Under Boltzmann equilibrium (no ss-RF) for a vector polarzation of 50% the resulting tensor polarization is,

$$P_{zz} = 2 - \sqrt{4 - 3P^2} = 19.7\%. \tag{64}$$

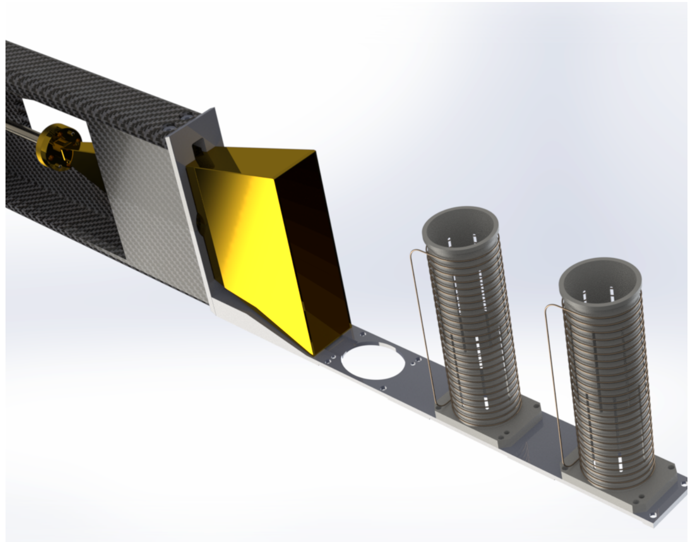

FIG. 19. Drawing of the ss-RF cup and coil used for the set of experiments discussed. The NMR coil is also shown inside. Figure from Carlos Ramirez of UVA polarized target group.

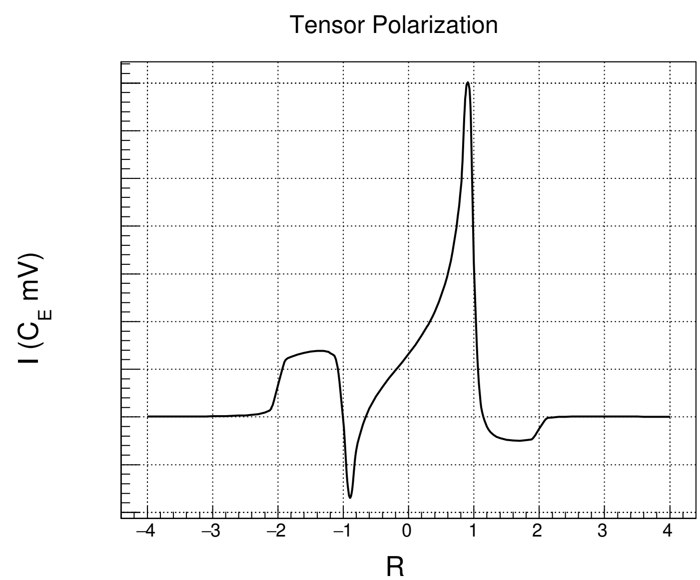

FIG. 20. The tensor polarization shown from the difference of the intensities $I_+(R)$ and $I_-(R)$. Figure from [112].

Enhancement beyond this level requires application of selective excitation [115] using the ss-RF to maximize the difference in the two intensities I_+ and I_- such that $P_{zz} = C(I_+ - I_-)$ is maximized.

Figure **??** shows a plot of the NMR lineshape for a vector polarization of 50%. This plot represents the sum of $I_+(R)$ and I_-(R) over the frequency domain in R. Similarly, a tensor polarization plot is shown in Figure 20 and represents the difference of $I_+(R)$ and $I_-(R)$ over the frequency domain in R. By selectively applying the ss-RF it is possible to reduce the regions in the P_{zz} line that drop below the x-axis. When this is done simultaneously over all negative regions in the domain the tensor polarization is enhanced.

5. Semi-Saturating RF Enhancement

To optimize the enhancement, the ss-RF excitation must minimize the negative tensor polarization for all R while minimizing the reduction to the overall area of the NMR signal from the process. The two critical regions lie around $R{\sim}{\mp}1$ ($\theta \approx \pi/2$) and $\pm 1 < R < \pm 2$ ($\theta \approx 0$). For positive vector polarization, the greatest integrated tensor polarization enhancement is achieved through selective excitation to reduce the size of the smaller transition area with intensity I_-. This can be thought of minimizing the negative parts of the tensor polarization, shown in Fig. 20. In both figures the y-axis would normally be millivolts scaled

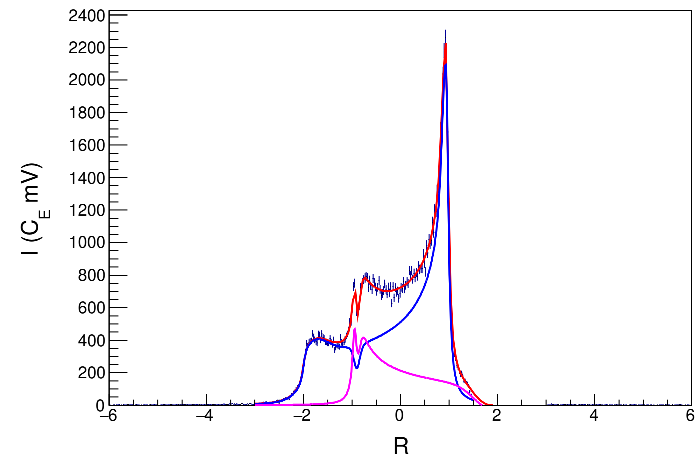

FIG. 21. NMR measurement with fit result after the ss-RF has been applied to the two negative tensor regions. The tensor polarization from this example is about 32%. Figure from [112].

by a multiplicative factor C_E which is sensitive to the characteristics of the NMR coil, such as inductance, geometry and orientation. We therefor leave these units generalized and provide a scale for relative change when necessary. For negative vector polarization, the greatest enhancement comes from the reduction of the transition area with intensity I_+, otherwise the treatment of both cases are identical, so it is convenient to focus on positive vector and tensor polarization.

The target must first be polarized with DNP to achieve the highest vector polarization possible for that material. This maximized the signal area to be used in the ss-RF manipulation.

The ss-RF is then applies as described. Because of the power amplification in the ss-RF damage to the Q-meter may result if these systems are ran simultaneously. Cycling between RF manipulation and NMR measurement can result in additional uncertainty in the NMR measurement due to the delayed sampling and the evolution of the spin state in the ensemble over time.

The ss-RF is applied by modulating the frequency over the domain of interest. The pedestal region of the smaller intensity (I_-) can be brought to near saturation to optimize. Saturation occurs when the RF drives the population of the magnetic sublevels to equalize. However, the peak is highly sensitive to power being it is higher in magnitude and it is necessary to preserve as much of the larger intensity (I_+) underneath the I_- peak as possible. Optimization requires just the right amount of RF power to reduce the area in I_- without depleting I_+.

To maximize tensor polarization first the DNP process is used to build up the available polarization as much as possible, then the can be optimized for either the vector polarization observable $A_T^{\sin(\varphi_{sc}-\varphi_c)}$ or the tensor polarized observable $A_{E_{xy}}$. Once the DNP process has maximize the NMR signal area (to around 50%), the the ss-RF is imposed to maximize tensor polarization. A fit to the data is also shown indicating the I_+ intensity in blue and the I_- intensity in pink. Figure 21 shows the NMR measurement after the ss-RF has been applied to the two negative tensor regions in R. A fit to the data is shown which uses only the constraints from Eq. 62 and Eq. 63 resulting in a tensor polarization measurement of about 30%. In optimal circumstances using a combination of AFP and ss-RF well over 30% tensor polarization can be achieved. Fortunately, as the target polarized decays due to radiation damage the enhancement potential per total NMR signal area increases. This is simply because the two peaks in the pake double become closer in area.

The same techniques that are used to enhance the tensor polarization can also be used to reduce it. This is done by applying the ss-RF to the larger peak and manipulating the signal so that I_- and I_+ are equal. The ss-RF manipulated signal lineshape is show in Fig. 22 for vector polarization of $P = 35\%$ and $P_{zz} = 0$.

The proposed experiment will take advantage of this novel polarized target system providing a farther physics reach by improving the figure of merit of the polarized observables and providing a method to disentangle the polarized neutron observables associated with quark transversity and the tensor polarized observable associated with gluon transversity. This is achieved best by polarizing under Boltzmann equilibrium then enhancing the tensor polarization and then polarizing with zero tensor polarization. The ss-RF manipulation can be done on the order of several seconds so these target spin flips can be done in between the beam spills and cycled to reduce the over all systematics.

6. *FNAL Auspicious Beam Cycle*

Fermilabs unique beam cycle from the Main Injector of 4.4 seconds of high intensity proton beam with 55.6 seconds before the next spill allows applications for polarized fixed target experiments not otherwise achievable. The superconducting polarizing magnet can not withstand such a continuous heat-load at such high beam intensity. We intend to run at the highest intensity that the spinQuest target magnet can withstand without creating local hot spots in the coils that go over the superconductor critical temperature resulting in magnet quenching. The time between spills allows for higher instantaneous intensity that

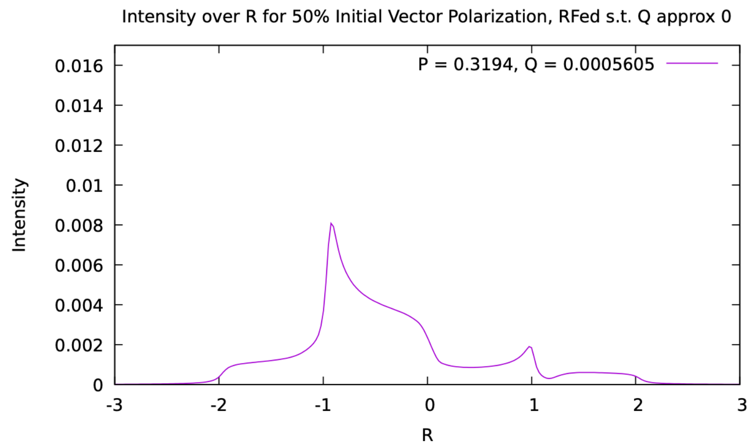

FIG. 22. The NMR lineshape for ss-RF manipulated deuteron signal with zero tensor polarization and roughly 35% vector polarization.

previously achieved by allowing time for the coil temperature to decrease back to baseline. That combined with the length (8 cm) of the SpinQuest target means that SpinQuest is operating at the polarized target *intensity frontier*.

The time between spills also allows for RF manipulation of the target spin configuration. The manipulation can be applied between the spill to prime the target for an enhanced state during the spill. Since these RF-generated spin states are not in thermal equilibrium, hold these states without decrease in polarization is not possible. The time between beam spills allows for recovery before the next spill. For this experiment tensor enhancement using a combination of AFP and ss-RF will increase the tensor polarization over the beam spill and then rebuild polarization when waiting for the next spill. This also makes it possible to cycle between a vector enhance target, a tensor enhanced and an unpolarized target for each still. This drastically reduces the uncertainty associated with time dependent drifts in the systematics.

Temporarily enhanced spin states during beam-target interactions are much more plausible at facilities that have a short beam spill per cycle such as Fermilab. The unique beam cycle of the high intensity proton beam at Fermilab allows for the employment of special characteristics of the thermal properties of the solid-state polarized target system allowing significant improvement over any other facility to run intense proton beams on novel RF-manipulated target systems. The combination of high luminosity, large x-coverage and a high-intensity beam with significant time between proton spills is paramount for this novel approach to measuring polarized target asymmetries in Drell-Yan scattering with high precision. This makes Fermilab very unique in this regard and allows great potential this proposal and for future projects.

7. *Kinematic Dilution Factor*

The figure of merit for this type of polarized target experiment is proportional to the active target contribution squared times polarization squared. The active target contribution is made of of the dilution factor and the packing fraction over the length of the target. The packing fraction can be measured using a method of cryogenic volume displacement measurement which compare an empty target cell to the full target cell used in the experiment. The target cell is filled with beads of solid NH_3 material with a typical packing factor of about 60% with the rest of the space filled with liquid helium.

The dilution factor is the ratio of the number of polarizable nucleons to the total number of nucleons in the target material and can be defined as,

$$f = \frac{N_D \sigma_{D,H}}{N_N \sigma_N + N_D \sigma_D + \Sigma N_A \sigma_A}, \tag{65}$$

where N_D is the number of deuteron nuclei in the target and σ_D is the corresponding inclusive double differential scattering cross section, N_N is the nitrogen number of scattered nuclei with cross section σ_N, and N_A is the numbers of other scattering nuclei of mass number A with cross section σ_A. The denominator of the dilution factor can be written in terms of the relative volume ratio of ND_3 to LHe in the target cell, the packing fraction p_f. For the case of a cylindrical target cell oriented along the magnetic field, the packing fraction is exactly equivalent to the percentage of the cell length filled with NH_3 or ND_3. The dilution factor for NH_3 is 0.176 and for ND_3 is 0.3. The uncertainty in these factors from irreducible background is typically 2-3%.

The material density for ND_3 is 1.007 g/cm^3 and a packing fraction higher than 0.06 can be achieved while the radiation length is about 5.7%. There are more materials in the experimental beam path than just the ND_3, which means the amounts and cross-sections of those materials must also be accounted for when calculating the kinematically sensitive dilution factor. Due to this, the dilution factor of the target will actually be given by the equation

$$f = \frac{3d^4\sigma_D^{DY}\left(x_B, x_T, \phi, \phi_T\right)}{\sum_A N_A d^4\sigma_A^{DY}\left(x_B, x_T, \phi, \phi_T\right)}. \tag{66}$$

Here A is required for each nuclei in the beam path. Background that are not from Drell-Yan must also be considered.

x_2-bin	$< x_2 >$	ND$_3$		ND$_3$+A		Full
		f	δf (%)	f	δf (%)	δf(%)
0.10 - 0.16	0.139	0.305	0.3%	0.310	0.6%	2.3%
0.16 - 0.19	0.175	0.304	0.5%	0.319	0.7%	2.4%
0.19 - 0.24	0.213	0.303	0.5%	0.327	0.7%	2.4%
0.24 - 0.60	0.295	0.306	1.6%	0.341	1.8%	2.5%

TABLE I. Here will list the dilution factor based on the MCFM simulations with kinematic sensitivity in x_2 for our four kinematic bins for pure deuterated ammonia (ND$_3$) as well as for the contribution from all materials (ND$_3$+A), as well as the total with contribution from packing fraction and target density in (Full). Errors contain contributions from both statistical and systematic uncertainty estimates.

To estimate the contribution from other materials in the beam path such as the aluminum windows, the target cell material, the NMR coils, the liquid Helium, and the target ladder, a cross-section generator called Monte Carlo Femtobarn (MCFM) [120] was used. The MCFM program is designed to calculate cross-sections based off of the parton distribution functions for various femtobarn-level processes in hadron-hadron collisions. A number of processes can be calculated at next-to-next-to-leading order in QCD. We use this software to estimate the Drell-Yan cross-section for our kinematics. Table I shows the resulting dilution factor from pure ND$_3$ as well as from the combination of all material in the beamline, shown in column (ND$_3$+A). The total percentage of dimuon yield is obtained by using the Geant4 with our target and spectrometer geometries constructed in the simulations. We also show the error estimate associated with relying purely on MCFM to provide the necessary cross-section to calculate the dilution factor for that kinematic bin. We also show in colomn (Full) the combined error estimation from MFCM, the target packing fraction and the ND$_3$ density.

V. BEAMLINE

The Neutrino-Muon (NM) beamline currently supporting the E906 Drell Yan experiment delivers a high-intensity (up to 10^{13} protons/4-sec spill), 120-GeV proton beam. The experimental beam has the 53 MHz microbunch characteristics of the Fermilab Main Injector RF structure and the longer microsecond structure of consecutively injected Fermilab Booster beam batches -with appropriate intervening kicker gaps separating the injected batches. After a lengthy beamline of a couple of kilometers interspersed with vacuum windows and in-beam diagnostics such as Secondary Emission Monitors (SEMs), the beam is distinctly Gaussian with Lorentzian tails. These tails are problematic for the cryogenic coils that polarize the E1039 target. However, this beamline is uniquely suited to tailor and customize beam properties - upstream beam collimation allows both matching the beam profile to the dimensions of the polarized target vertically and horizontally and protection against a quench of the SC magnet without creating increased backgrounds at the experiment.

A. Current and Proposed Beamline Configuration

The beam is slow-spill extracted from the Fermilab Main Injector on the half integer resonance and travels a couple of kilometers to the E906 target area in NM3. Losses in the couple of hundred meters upstream of the target are on the percent level and large backgrounds are not created in the experimental area. Although slow spill produces an asymmetric, non-elliptical phase space in the horizontal plane, after traveling through vacuum windows, diagnostics, and other sources of scattering, the beam in both planes becomes Gaussian-like (with Lorentzian tails) and even symmetry. (The vertical split of beam to the MTEST and MCENTER lines is at such low intensity, that the beam profile in this high-intensity line is not observably impacted.) The NM/E906 beam properties have been extensively studied to determine how to achieve the requested beam profile on the polarized target. A minimal spot size of $\sigma = 3 - 4$ mm is the smallest obtainable in both planes simultaneously with the present beamline magnet configuration and distances involved - the polarized target is 2 meter supstream of the current E906 targets so these measurements apply. The new experiment has requested a spot size of 6 - 7 mm. No magnet reconfiguration or additions are required with beam collimation, greatly reducing the cost and lab resources required. The present beamline magnet configuration can thus be used for the E1039 experiment. The primary modification required is to collimate beam tails by at least $\sim$ 10-20%, well upstream of the polarized target, to remove the potential for quenching the superconducting magnet and also to more evenly distribute beam across the target. To do this the NM2 target pile from the kTeV experiment will be used to absorb beam scattered by collimators (Palmer-style) positioned upstream of this pile. These collimators are currently stored downstream of the target pile but can be rigged around the shielding and installed upstream replacing two of the 5 4Q120s (only the two last quadrupoles, 3 and 4 are currently in use for E906).

By installing the collimators upstream, the beam can be collimated and tails clipped, scattered and completely absorbed by the NM2 target pile with little background reaching the experiment. A MARS study is planned for this configuration. Finally, a fixed collimator in the NM3 enclosure will shadow the SC coils of the polarized target to protect it not only from any residual halo but also beam steering allowing target scans.

The present E906 beamline is ideal for the proposed E1039 experiment, and especially for a polarized target. No modification to the present beamline magnet component configuration or new optics is required outside of replacing two NM2 4Q120s (not in service) with collimators. These collimators are available and already located within the NM2 enclosure so no extensive rigging and drop hatch work is required. This beamline represents the most cost effective approach to the proposed polarized target Drell Yan Experiment.

VI. COUNT RATES AND STATISTICAL ERRORS

The total Drell-Yan count rates on different targets are calculated using both full GEANT4 based Monte Carlo simulation program with Drell-Yan signal events generated by the NLO calculations done by Vitev, et. al., and the demonstrated performance of the Fermilab Main Injector combined with the E906/SeaQuest spectrometer.

Unlike E906/SeaQuest, the primary physics interest of E1039 experiment is to measure the low-x_2 range of polarized Drell-Yan production. We moved our target position from -130 cm to -300 cm, which greatly improves the low-x_2 acceptance and the triggering capability, as well as the offline target/dump separation power.

One primary bottleneck of the data collection efficiency at E906/SeaQuest is the slow Data Acquisition System (DAQ). A very tight trigger level selection has been implemented in E906/SeaQuest so as to accommodate as many events in our limited DAQ bandwidth as possible. In the summer shutdown between Run-IV (FY-2016) and Run-V (FY-2017), we will be upgrading our DAQ system to increase the bandwidth by a factor of 10, which will be available for the last run of E906/SeaQuest and following experiments.

Another limiting factor of the data collection efficiency at E906/SeaQuest is the unstable instantaneous beam intensity, which is sometimes more than one order of magnitude larger than average. To prevent the spectrometer from being completely saturated, the total number of protons delivered to the target has to be limited to be less than 6×10^{12} per spill, to indirectly constrain the instantaneous beam intensity. This also requires the data taking to be inhibited on all neighboring RF buckets when a high intensity bucket arrives. After careful optimization, E906/SeaQuest has been able to record on average 2.67×10^{12} protons per spill, which corresponds to 7.7×10^{17} protons per calendar year.

After running for 2 years with beam time evenly split on NH_3 and ND_3 targets the integrated luminosity on NH_3 (ND_3) target is expected to be $1.82 \times 10^{42} (2.11 \times 10^{42})$ cm^{-2}. With the various assumed efficiencies shown in Table II, the final event yield and statistical precision of A_N measurement in each x_2 bin is summarized in Table III. Here the statistical precision is calculated by $\Delta A_N = \frac{1}{f}\frac{1}{P}\frac{1}{\sqrt{N}}$, where f denotes the dilution factor, P denotes the average polarization, and N denotes the event yield in each x_2 bin.

Sources	Target/Accelerator	Spectrometer	Acceptance	Trigger	Reconstruction
Efficiency (%)	50	80	2.2	90	60

TABLE II. Various efficiencies assumed for the count rate estimates based on previous experience with E906 and polarized target operations.

x_2-bin	$< x_2 >$	Vector-NH_3 ($d^{\uparrow}$)		Tensor-ND_3 ($d^{\uparrow}$)		$n^{\uparrow}$
		N	$\Delta A_{E_{xy}}$ (%)	N	$\Delta A_{E_{xy}}$ (%)	ΔA_T^{sin}(%)
0.10 - 0.16	0.139	3.0×10^4	4.7	3.8×10^4	4.3	6.3
0.16 - 0.19	0.175	2.7×10^4	5.2	3.2×10^4	4.6	6.6
0.19 - 0.24	0.213	4.3×10^4	5.5	3.9×10^4	4.1	6.1
0.24 - 0.60	0.295	3.3×10^4	5.3	3.8×10^4	4.1	6.2

TABLE III. Event yield and statistical precision of the A_N measurement in each of the x_2 bins for the vector polarized NH_3 ($d^{\uparrow}$) and the tensor polarized ND_3 ($d^{\uparrow}$) targets as well as the deduced A_N measurement precision for polarized n.

A. Target Polarization Uncertainty

The lower limit for polarization uncertainty is set by the Q-meter style NMR which can not be expected to preform better that 1% relative error. UVA test lab studies have gone down as far as 1.5% but typically in an experiment 2-4% is achieved for the proton. The Deuteron/neutron has much larger error but with the use of the cold NMR system [110, 115] in combination with the multiple measurement techniques it is also possible to get down into the same uncertainty region as the proton.

VII. LUMINOSITY AND BEAM INTENSITY

A. Beam Profile

The typical profile of the beam delivered to the target is a two dimensional Gaussian with a width of $\sigma_x = 6.8$ mm, $\sigma_y = 7.6$ mm. The beam will be clipped with collimators at $\pm 1.25\sigma$, giving a beam profile of $\Delta x = 17$ mm, $\Delta y = 19$ mm. The beam is expected to drift no more than ± 2 mm in the x-direction before collimation. The change of the luminosity of the beam due to the beam drifting is $(N_{beam} - N_{drift})/N_{beam}$. The change in the delivered Luminosity is $\Delta\mathcal{L} = 2.8\%$.

B. Luminosity measurement

Several detector and measurement techniques are used in order to control systematic uncertainties from changing beam conditions, such as position, luminosity and shape. The absolute beam intensity will be determined by Unser Monitors, which are upstream of the target. The accuracy of Unser Monitors has been established to be 0.05% [118].

Four detectors at 90° to the beam (two horizontally and two vertically) will help monitor the instantaneous luminosity. Each of these detectors will consist of four plastic scintillators in coincidence and positioned outside of the shielding wall, pointing through a small hole in the shielding at the target. Fast MC simulations show that these detectors will detect normal $\pi^{\pm}$s, $\mu^{\pm}$s, γs with $E > 100$ MeV on the order of $\sim$200 kHz.

The ratio of every one of these detectors over the Unser Monitor measurement (N_{90°/N_{unser}) will provide a fast relative luminosity measurement. If part of the beam profile deviates off the target after the Unser measurement, the 90° detectors will be able detect luminosity changes to >1%. This error comes from the efficiency of the four fold coincidence scintillators in each 90° detector. If each scintillator paddle is $\epsilon_{scint} = 99.8\%$ efficient, the total efficiency goes as $\epsilon^4_{scint} \approx 99\%$.

As an additional check on the relative beam intensity, a four plate RF cavity will be installed, which can also determine relative changes in the beam position, $N_{90^\circ}/N_{RF} \propto (N_{90^\circ}/N_{unser})$.

C. Consistency in Delivered Luminosity

Since extracting the Sivers asymmetry for the $d(\bar{x})$ requires to measure the ratio of $\frac{\sigma^{pd}}{2\sigma^{pp}}$, care has to be taken that the running conditions for both targets are as identical as possible. Our target system will have three identical cells, two filled with NH_3 and the other with ND_3, or vice-versa. These will be interchanged on a regular basis to minimize systematic effects.

Finally, a fourth cell will have an empty cell for background subtraction, which can be replaced with a Carbon disk, to study false asymmetries.

VIII. OVERALL SYSTEMATIC ERROR

The following table lists estimates of the dominant contributions to the relative systematic error as described in the text.

Quantity	Error
Polarization Measurement	2.5%
Dilution Factor	2.5%
DAQ and Dead Time	1.5%
Relative Luminosity	1 %

TABLE IV. *Estimates for the systematic errors*

Adding these numbers, we estimate our relative systematic error to be less than 4%. We also expect an absolute systematic error due to the muon spectrometer of <1.0%.

IX. EXPECTED RESULTS

In Fig 24 we show the expected results after two years of running with both NH_3 and ND_3 targets. The errors displayed are the statistical precision as listed in Table III, while the expected systematic uncertainty is discussed in the caption. The calculations are based on global fits to the available SIDIS data. The large discrepancy is a reflection of the fact that the current SIDIS data are insensitive to the seaquark contribution, thus leading to large uncertainties in the calculations. This is also reflected in the width of the uncertainty bands.

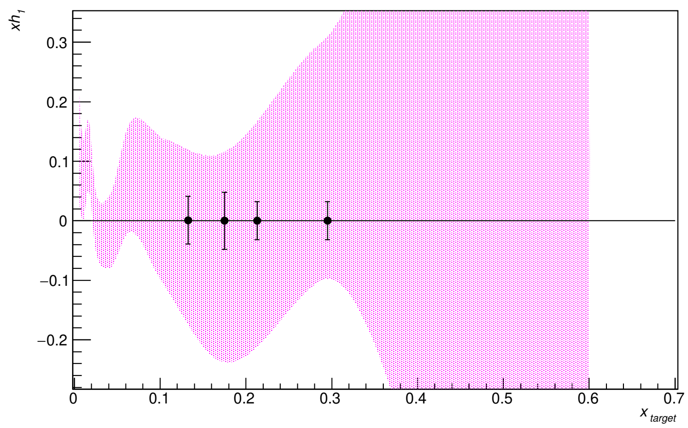

FIG. 23. Expected results after two years of running on NH_3 and ND_3 targets. The red error bars are statistical only. Absolute systematic uncertainty is estimated to be <1.0% (see Sec. **??**), and the relative systematic uncertainty is 4.0%. The theory model predictions are for NH_3 target only.

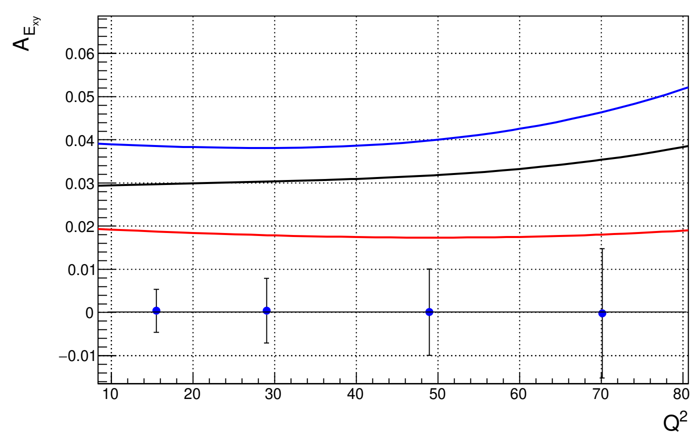

FIG. 24. Projections of the gluon transversity asymmetry with expected data point. Error bars on projected data points are from statically and systematic uncertainty estimates.

From the analytical scope of QCD there is a certain ubiquity of gluons to consider in almost any relevant process. However probing the gluonic structure of hadrons and nuclei is considerably more difficult than that of quarks. To some extent that can be accredited to the significant innate challenges in measurements of gluon observables which are usually $\mathcal{O}(\alpha_s)$-suppressed relative to the quark observables. Here we suggest a measurement that can provide significant information. A finite value of the gluon h_{1TT} is likely to trigger a multitude of new experiments to probe the full kinematic range of this observable to help map out and detail the relationship between the nuclear geometry and the gluonic structure. It has also been suggested [119] that the magnitude of this observable should increase with atomic number (z). There is ongoing polarized target research [121] to polarized higher z solid-state targets.

[1] J. Ashman *et al.* Nucl. Phys. B 328,1 (1989).
[2] S. D. Bass, Rev. Mod. Phys.77, 1257 (2005) [hep-ph/0411005].
[3] M. Burkardt, C. A. Miller and W. D. Nowak, Rept. Prog. Phys.73, 016201 (2010).
[4] S. E. Kuhn, J.-P. Chen and E. Leader, Prog. Part. Nucl. Phys.63, 1 (2009).
[5] J. P. Chen, Int. J. Mod. Phys.E19, 1893 (2010).
[6] J. Blumlein, Prog. Part. Nucl. Phys.69, 28 (2013) [arXiv:1208.6087 [hep-ph]].
[7] P. Hoodbhoy, X. Ji Nucl. Phys. Rev. D60 (1999) 114042.
[8] B. Lee *et al.* Inter. J. Mod. Phys. A Vol. 32, No. 11, 1750062 (2017).
[9] R. P. Feynman, Phys. Rev. Lett.23, 1415 (1969); J. D. Bjorken, and E. A. Paschos, Phys. Rev.185, 1975 (1969).
[10] M. Diehl Eur.Phys.J. A52 (2016) no.6, 149 arXiv:1512.01328 [hep-ph] DESY-15-234.
[11] H.-W. Lin, R. Gupta, B. Yoon, Y.-C. Jang and T. Bhattacharya, Phys. Rev.D98(2018) 094512.
[12] C. Alexandrou, M. Constantinou, K. Hadjiyiannakou, K. Jansen, C. Kallidonis, G. Koutsou et al.,Phys. Rev. Lett.119(2017) 142002.
[13] J. Liang, Y.-B. Yang, T. Draper, M. Gong and K.-F. Liu,Phys. Rev.D98(2018) 074505.
[14] M. Engelhardt, Phys. Rev.D86(2012) 114510.
[15] C. Alexandrou, M. Constantinou, K. Hadjiyiannakou, K. Jansen, H. Panagopoulos and C. Wiese, Phys. Rev.D96(2017) 054503.
[16] Jian-Hui Zhang *et al.*, Phys. Rev.D100, 034505 (2019).
[17] R. Gupta, Proc. of Sci. SPIN2018 10-14 September, 2018LA-UR-19-22704, arXiv:1904.00312.
[18] H.-W. Lin, R. Gupta, B. Yoon, Y.-C. Jang and T. Bhattacharya, Phys. Rev.D98 (2018) 094512[1806.10604].
[19] C. Adolph *et al.* (COMPASS Collaboration), Phys.Lett. B717, 376 (2012), arXiv:1205.5121 [hep-ex].
[20] C. Alexandrou, M. Constantinou, K. Hadjiyiannakou, K. Jansen, C. Kallidonis, G. Koutsou et al., Phys. Rev. Lett.119(2017) 142002[1706.02973].
[21] M. Engelhardt, J. Green, N. Hasan, S. Krieg, S. Meinel, J. Negele et al., PoSSPIN2018(2019) 047[1901.00843].
[22] R. L. Jaffe, Int. J. Mod. Phys. A18 (2003) 1141-1152, arXiv:hep-ph/0201068.
[23] Leader E., Anselmino M.Z. Phys. C, 1988, v. 41, 239.
[24] J. P. Ralston and D. E. Soper, Nucl. Phys. B 152, 109 (1979).
[25] X. Artru and M. Mekhfi, Z. Phys. C 45, 669 (1990).
[26] R. L. Jaffe and X. D. Ji, Nucl. Phys. B 375, 527 (1992).
[27] V. Barone, A. Drago, and P. G. Ratcliffe, Phys. Rept. 359, 1 (2002). arXiv:hep-ph/0104283 [hep-ph].
[28] V. Barone and R. G. Ratcliffe, (World Scientific, Singapore, 2003).
[29] M. Radici and A. Bacchetta, Phys. Rev. Lett. 120, 192001 (2018).
[30] S. Kumano and M. Miyama, Phys. Rev. D 56, R2504 (1997).
[31] A. Hayashigaki *et al.*, Phys. Rev. D 56, 7350 (1997).
[32] W. Vogelsang, Phys. Rev. D 57, 1886 (1998).
[33] J. L. Forest *et al.* Phys. Rev. C54,646-667 (1996).
[34] R. L. Jaffe, A. Manohar, Phys. Lett. B 223 (1989) 218-224.
[35] A. Klein, D. Keller and K. Liu, E1039 proposal, SEAQUEST Document 1720-v3.
[36] SD. Drell and TM. Yan, Phys. Rev. Lett.25(1971) 316.
[37] S. Arnold, A. Metz, and M. Schlegel, Phys. Rev. **D79**, 034005 (2009), arXiv:0809.2262 [hep-ph]
[38] S. Hino and S. Kumano, Phys. Rev. D 60, 054018 (1999).
[39] S. Hino and S. Kumano, Phys. Rev. D 59, 094026 (1999)
[40] S. Kumano and Qin-Tao Song, KEK-TH-1953, J-PARC-TH-0082, arXiv:1702.01477
[41] S. Kumano and M. Miyam, Phys. Lett. B 479 2000 149–155
[42] S. Kumano and Qin-Tao Song, Phys. Rev. D94, 054022 (2016)
[43] S. Kumano and Qin-Tao Song, KEK-TH-2111, J-PARC-TH-0163, arXiv:1910.12523
[44] A. Sissakian, O. Shevchenko, A. Nagaitsev and O.Ivanov Physics of Particles and Nuclei volume 41, pages64–100 (2010).
[45] A. Sissakian, O. Shevchenko, A. Nagaytsev, and O. Ivanov, Eur. Phys. J. C 59 (2009) 659-673.
[46] A. N. Sissakian, O. Y. Shevchenko, A. P. Nagaytsev and O. N. Ivanov, Phys. Rev. D 72, 054027 (2005).
[47] D. Boer, S. Cotogno, T. van Daal, P.J. Mulders, A. Signori and Y.-J. Zhou, JHEP10(2016) 013, arXiv:1607.01654 [hep-ph]
[48] J. Matousek, COMPASS Thesis 2018 http://wwwcompass.cern.ch/compass/publications/theses/2018_phd_matousek.pdf
[49] M. Boglione and A. Prokudin, Eur. Phys. J. **A52** (2016) 154, arXiv:1511.06924.
[50] A. Bacchetta and P.J. Mulders, Phys. Rev.D 62(2000) 114004
[51] R. L. Jaffe, arXiv:hep-ph/9602236, in The Spin Structure of the Nucleon: International School of Nucleon Structure, edited by B. Frois et al. (World Scientific, 1997).
[52] S. Cotogno, TV. Daal and P. Mulders, JHEP11 (2017) 185
[53] J. Collins and J.-W. Qiu, Phys. Rev. D75 (2007) 114014, arixiv: 0705.2141 [hep-ph]
[54] D. Boer, S. J. Brodsky, P. J. Mulders and C. Pisano, Phys.Rev.Lett. 106 (2011) 132001, [1011.4225].
[55] T. C. Rogers and P. J. Mulders, Phys. Rev. D81 (2010) 094006, [1001.2977].
[56] P. J. Mulders and T. C. Rogers, Gauge Links, TMD-Factorization, and TMD-Factorization Breaking, 1102.4569.
[57] T. C. Rogers, Phys. Rev. D88 (2013) 014002, [1304.4251].
[58] C. J. Bomhof and P. J. Mulders, Non-universality of transverse momentum dependent parton distribution functions, Nucl. Phys. B795 (2008) 409–427, [0709.1390].

[59] D. Boer, C. Lorc e, C. Pisano and J. Zhou, Adv. High Energy Phys. 2015 (2015) 371396, [1504.04332].
[60] J.-W. Qiu and G. Sterman, Phys. Rev. Lett. 67 (1991) 2264–2267.
[61] J.-W. Qiu and G. Sterman, Phys. Rev. D59 (1999) 014004, [hep-ph/9806356].
[62] D. Keller, FNAL-SpinQuest Letter of Intent (*Longitudinal Structure of the Deuteron in Drell-Yan*) In Progress (2020).
[63] J. C. Collins, Nucl. Phys. B396, 161 (1993), arXiv:hep-ph/9208213
[64] J. Collins, Phys. Lett. **B536**, 43 (2002), arXiv:hep-ph/0204004 [hep-ph]
[65] A. Airapetian et al. (HERMES), Phys. Rev. Lett. 94, 012002 (2005), hep-ex/0408013.
[66] A. Airapetian et al. (HERMES), Phys. Lett. B693, 11 (2010), arXiv:1006.4221 [hep-ex].
[67] X. Qian et al. (Jefferson Lab Hall A Collaboration), Phys.Rev.Lett. 107, 072003 (2011), arXiv:1106.0363 [nucl-ex].
[68] K. Abe et al. (Belle), Phys. Rev. Lett. 96, 232002 (2006), arXiv:hep-ex/0507063 [hep-ex].
[69] R. Seidl et al. (Belle), Phys. Rev. D78, 032011 (2008), arXiv:0805.2975 [hep-ex].
[70] I. Garzia (BaBar), PoS ICHEP2012, 272 (2013), arXiv:1211.5293 [hep-ex].
[71] A. Metz, Phys. Lett. B549, 139 (2002), hep-ph/0209054.
[72] M. Radici, A. Courtoy, A. Bacchetta, and M. Guagnelli, (2015), arXiv:1503.03495 [hep-ph].
[73] Zhong-Bo Kang, et al. JLAB-THY-15-2044, arXiv:1505.05589v1 [hep-ph]
[74] D. de Florian, R. Sassot, M. Stratmann, and W. Vogelsang, Phys.Rev. D80, 034030 (2009), arXiv:0904.3821 [hep-ph].
[75] J. Soffer, Phys. Rev. Lett. 74, 1292 (1995), hep-ph/9409254.
bibitemanna A. Martin, F. Bardamante, and V. Barone, Phys. Rev. D 91, 014034 arXiv:1412.5946v2 [hep-ph]
[76] M. Radici and A. Bacchetta, Phy. Rev. Let. 120, 192001 (2018).
[77] M. Cirelli, E. Del Nobile, P. Panci, JCAP 1310 (2013) 019. arXiv:1307.5955.
[78] T. Bhattacharya, V. Cirigliano, S. D. Cohen, A. Filipuzzi, M. Gonzalez-Alonso, et al., Phys.Rev. D85 (2012) 054512. arXiv:1110.6448.
[79] A. Courtoy, S. Baeler, M. Gonzlez-Alonso, S. Liuti, Beyond-Standard-Model Tensor Interaction and Hadron Phenomenology, Phys. Rev. Lett. 115 (2015) 162001. arXiv:1503.06814.
[80] J.Green, J.Negele, A.Pochinsky, S.Syritsyn, M.Engelhardt, et al., Phys.Rev. D86 (2012) 114509. arXiv:1206.4527.
[81] T. Bhattacharya, S. D. Cohen, R. Gupta, A. Joseph, H.-W.Lin, et al., Phys.Rev. D89 (9) (2014) 094502. arXiv:1306.5435.
[82] T.Bhattacharya, V.Cirigliano, S.Cohen, R.Gupta, H.-W.Lin, B.Yoon, Axial, Scalar and Tensor Charges of the Nucleon from 2+1+1-flavor Lattice QCD arXiv:1606.07049.
[83] J.-W. Chen, S. D. Cohen, X. Ji, H.-W. Lin, J.-H. Zhang, Nucl. Phys. B911 (2016) 246–273. arXiv:1603.06664, doi:10.1016/j.nucl phys b.2016.07.033.
[84] G. S. Bali, S. Collins, B. Glssle, M. Gckeler, J. Najjar, etal. Phys.Rev.D91(5)(2015) 054501. arXiv:1412.7336.
[85] R. Gupta, T. Bhattacharya, A. Joseph,H.-W.Lin, B.Yoon, PoSLattice2014v(2014)v152. arXiv:1501.07639.
[86] N. Yamanaka, H. Ohki, S. Hashimoto, T. Kaneko, PoS LATTICE2015 (2016) 121. arXiv:1511.04589.
[87] Y.Aoki, T.Blum, H.-W.Lin, S.Ohta, S.Sasaki,etal., Phys.Rev. D82 (2010) 014501. arXiv:1003.3387.
[88] M. Gockeler, et al., Phys.Lett. B627 (2005) 113–123. arXiv:hep-lat/0507001, doi:10.1016/j.physletb.2005.09.002.
[89] N. Yamanaka, T. M. Doi, S. Imai, H. Suganuma, Phys. Rev. D88 (2013) 074036. arXiv:1307.4208, doi:10.1103/PhysRevD.88.074036.
[90] M. Pitschmann, C.-Y. Seng, C. D. Roberts, S. M. Schmidt, Phys.Rev. D91 (7) (2015) 074004. arXiv:1411.2052, doi:10.1103/PhysRevD.91.074004.
[91] A. Czarnecki and B. Krause, Phys. Rev. Lett. 78, 4339 (1997).
[92] M. B. Hecht and B. H. J. McKellar, Phys. Rev. C 60, 065202 (1999).
[93] M. B. Hecht, C. D. Roberts, and S. M. Schmidt, Phys. Rev. C 64, 025204 (2001).
[94] T. Liu, Z. Zhao, and H. Gao, Phys. Rev. D 97, 074018 (2018).
[95] M. Pospelov and A. Ritz, Ann. Phys. (Amsterdam) 318, 119 (2005).
[96] T. E. Chupp, P. Fierlinger, M. J. Ramsey-Musolf, and J. T. Sigh, Rev. Mod. Phys. 91, 015001 (2019).
[97] S. Kumano and Qin-Tao Song, Phys. Rev. D 101, 054011 (2020).
[98] J.P. Ralston, D. E. Soper, Production of dimuons from high-energy polarized proton-proton collisions, Nucl. Phys. B152 (1979) 109.9
[99] R.L. Jaffe, X.Ji, Chiral odd parton distributions and polarized Drell-Yan, Phys. Rev. Lett. 67 (1991) 552–555.
[100] J. L. Cortes, B. Pire, J. P. Ralston, Measuring the transverse polarization of quarks in the proton, Z. Phys. C55 (1992) 409–416. doi: 10.1007/BF01565099.
[101] V.Barone, A.Drago, P. G. Ratcliffe, Transverse polarisation of quarks in hadrons, Phys. Rept. 359 (2002) 1–168. arXiv:hep-ph/0104283.
[102] D. Boer, M. Diehl, R. Milner, R. Venugopalan, W. Vogelsang, et al., Gluons and the quark sea at high energies: Distributions, polarization, tomography arXiv:1108.1713.
[103] J. Dudek, R. Ent, R. Essig, K. Kumar, C. Meyer, et al., Physics Opportunities with the 12 GeV Upgrade at Jefferson Lab, Eur.Phys.J. A48 (2012) 187. arXiv:1208.1244, doi:10.1140/epja/i2012-12187-1.
[104] A. Accardi, J. Albacete, M. Anselmino, N. Armesto, E. Aschenauer, et al., Electron Ion Collider: The Next QCD Frontier - Understanding the glue that binds us all. arXiv:1212.1701.
[105] NIM article accepted to publish https://arxiv.org/abs/1706.09990
[106] D. Crabb, and W. Meyer, Ann. Rev. Nucl. Part. Sci. 47:67-109 (1997)
[107] D. G. Crabb, *et al.* Phys. Rev. Let. 64: 2627-2629 (1990)
[108] G.R. Court, *et al.*, Nucl. Instr. Meth. in Phys. Res. A 324 433 (1993)
[109] O. Kahn, Molecular Magnetism, VCH, New York (1993)
[110] D. Keller, Nucl. Instr. Meth. A728 133 (2013)
[111] G. Court, M. Houlden, S. Bultmann, D. Crabb, D. Day, Y. Prok et al., Nucl. Instr. Meth. in Phys. Res. A 527 (2004) 253.

[112] D. Keller, *et al.*, Nucl. Instr. Meth. in Phys. (submitted).
[113] G. E. Pake, J. Chem. Phys. 16, 327 (1948)
[114] C. Dulya, *et al.*, NIM A 398 109-125 (1997)
[115] D. Keller, Eur. Phys. J. A 53, 155 (2017) arXiv:1707.07065
[116] C. D. Jeffries, Dynamic Nuclear Orientation, Interscience Publishers, New York (1963)
[117] P.P.J Delheij, D.C. Healey, and G.D. Wait, Nucl. Instr. and Meth. A251 498-510 (1986)
[118] K. B. Unser, AIP Conf. Proc. 252, 266 (1992)
[119] P. Hoodbhoy, *et al.*, Nucl. Phys. B312, 571 (1989)
[120] R. Boughezal, J. M. Campbell, R. K. Ellis, C. Focke, W. Giele, X. Liu, F. Petriello and C. Williams, arXiv:1605.08011 [hep-ph].
[121] D. Keller, Recent work at UVA, Tensor Polarized Solid Target Workshop, March 10-12, 2014
[122] D. Keller, Rotating Polarized Target Systems, NPS-CPS Collaboration Meeting, Jan. 28, 2017